AD NUMBER

AD814721

NEW LIMITATION CHANGE

TO

Approved for public release, distribution unlimited

FROM

Distribution authorized to U.S. Gov't. agencies only; Specific Authority; 13 Jan 1967. Other requests shall be referred to Secretary of the Army, Office of Civil Defense, Washington, DC.

AUTHORITY

DCPA ltr, 30 Nov 1972

GENERAL ATOMIC
DIVISION OF GENERAL DYNAMICS

GA-7597
OCD Work Unit # 3111A

CLOUD CHEMISTRY OF FALLOUT FORMATION

FINAL REPORT

by

J. H. Norman and P. Winchell

Prepared for
Office of Civil Defense
Secretary of the Army
Department of Defense, 20301
under
Contracts N228-(62479)67968 and NOO22866 C0403
through the
U. S. Naval Radiological Defense Laboratory
San Francisco, California 94135

January 13, 196[illegible]

CLOUD CHEMISTRY OF FALLOUT FORMATION. FINAL REPORT
OCD Work Unit #3111A--GA

GENERAL ATOMIC

DIVISION OF

GENERAL DYNAMICS

JOHN JAY HOPKINS LABORATORY FOR PURE AND APPLIED SCIENCE

P.O. BOX 608, SAN DIEGO, CALIFORNIA 92112

GA-7597
OCD Work Unit # 3111A

CLOUD CHEMISTRY OF FALLOUT FORMATION

FINAL REPORT

by

J. H. Norman and P. Winchell

Performed for
Office of Civil Defense
Secretary of the Army
Department of Defense, 20301
under
Contracts N228-(62479)67968 and NOO22866C0403
through the
U. S. Naval Radiological Defense Laboratory
San Francisco, California 94135

January 13, 1967

CONTENTS

SUMMARY vii

INTRODUCTION 1

STUDIES OF HENRY'S LAW CONSTANTS 3
- Introduction 3
- Experimental Studies of Cesium and Rubidium 4
- Other Studies 12

DIFFUSION OF RADIONUCLIDES IN MOLTEN SILICATES 15
- Introduction 15
- Methods 15
- Results 16
- Discussion 19

STUDIES OF THE THERMODYNAMIC PROPERTIES OF GASEOUS SPECIES 39
- Introduction 39
- Gaseous Alkali Metal Oxides 39
- Cesium Silicate Studies 41
- Cerium Oxide Studies 41

A CONDENSED STATE, DIFFUSION-LIMITED MODEL OF FISSION PRODUCT ABSORPTION IN FALLOUT 43

ELECTRON MICROPROBE STUDIES 47

PARTICLE LEACHING STUDIES 73
- Simulated Fallout Studies 73
- Fallout Particle Studies 77
- Cloud Chemistry Phenomenology 78

REFERENCES 79

FIGURES

1. Universal curve for transpiration studies with gaseous diffusion in the capillary 5

2. Transpiration apparatus 7

3. Cesium transpiration from $CaO-Al_2O_3-SiO_2$ eutectic at 1785°K (P_{O_2} = 1 atm) 8

4. Rubidium transpiration from $CaO-Al_2O_3-SiO_2$ eutectic at 1641°K (P_T = 1 atm) 9

5. Cesium vapor pressure per molten $CaO-Al_2O_3-SiO_2$ eutectic loading as a function of reciprocal temperature 10

6. Rubidium vapor pressure per molten $CaO-Al_2O_3-SiO_2$ eutectic loading as a function of reciprocal temperature 11

7. Example of the penetration data from the plane-source technique for radiotin transport in the 1450°K eutectic of the $CaO-Al_2O_3-SiO_2$ ternary at 1858°K 17

8. Example of data from the vaporization technique for radiorubidium transport in the 1450°K eutectic of the $CaO-Al_2O_3-SiO_2$ ternary at 1722°K 18

9. Diffusivities for transport of radioiodine in 1450°K eutectic $CaO-Al_2O_3-SiO_2$ using the vaporization technique 20

10. Diffusion coefficients for transport of radiocesium in a molten $CaO-MgO-Fe_2O_3-Al_2O_3-SiO_2$ matrix using the plane-source technique. The low temperature sample was devitrified 21

11. Diffusion coefficients for transport of radiorubidium in molten eutectic $CaO-Al_2O_3-SiO_2$ 22

12. Diffusion coefficients for transport of radiopotassium in molten eutectic $CaO-Al_2O_3-SiO_2$ using the plane-source technique 23

13. Diffusion coefficients for transport of radioindium in molten eutectic $CaO-Al_2O_3-SiO_2$ using the plane-source technique . . . 24

14. Diffusion coefficients for transport of radiotin in molten eutectic $CaO-Al_2O_3-SiO_2$ using the plane-source technique 25

15. Diffusion coefficients for transport of radiosodium in molten eutectic $CaO-Al_2O_3-SiO_2$ using the plane-source technique 26

16. Diffusion coefficients for transport of radiocesium in molten eutectic $Na_2O-Al_2O_3-SiO_2$. The dashed curve is an extrapolation of previously reported diffusivity in eutectic $CaO-Al_2O_3-SiO_2$ 27

17. A:B correlation for diffusion in molten silicates obtained in this laboratory 28

18. Correlation between the coefficients in the diffusion equation, $\log D = A - BT^{-1}$, for diffusion of nuclides in silicates 30

19. Example of the compensation law. Diffusion of various metals in copper. Data taken from Ref. 8 32

20. Correlation of coefficients in the diffusion equation, $\log D = A - BT^{-1}$, with reciprocal ionic radius for diffusion of cesium, rubidium, potassium, and sodium in molten eutectic $CaO-Al_2O_3-SiO_2$ 34

21. Correlation between A in $\log D = A - BT^{-1}$ with reciprocal effective ionic radius for diffusion in the 1450°K eutectic of the $CaO-Al_2O_3-SiO_2$ ternary 35

22. Correlation between A in $\log D = A - BT^{-1}$ with reciprocal effective ionic radius for a low refractory silicate glass. Data taken from Ref. 10 37

23. Photographs of a sectioned irregular particle: (a) photomicrograph; (b) electron back scatter picture, field ~250μ × 250μ (all microprobe pictures are this field unless otherwise stated); (c) Fe K_α picture 49

24. Fe K_α picture of a sectioned irregular particle 51

25. Photographs of a sectioned "spheroidal ceramic" particle: (a) microphotograph; (b) electron back scatter picture; (c) Fe K_α picture 52

26. Photographs of a sectioned "spheroidal ceramic" particle: (a) microphotograph; (b) Ca K_α picture; (c) Fe K_α picture 53

27. Photographs of a sectioned "spheroidal ceramic" particle: (a) microphotograph; (b) electron back scatter picture; (c) Ca K_α picture 54

28. Electron back scatter picture of a sectioned "spheroidal ceramic" particle 55

29. Photographs of a sectioned black spheroidal particle: (a) microphotograph; (b) Ca K_α picture; (c) Fe K_α picture; (d) Si K_α picture 58

30. Photographs of a sectioned black spheroidal particle: (a) microphotograph; (b) Ca K_α picture; (c) Fe K_α picture; (d) Si K_α picture 59

31. Photographs of a sectioned dendritic black spheroidal particle: (a) microphotograph; (b) Ca K_α picture; (c) Fe K_α picture; (d) Si K_α picture; (e) Zr L_α picture; (f) Ti K_α picture; (g) Ba L_α picture; (h) S K_α picture; (i) Cl K_α picture; (j) K K_α picture 60

32. Photographs of a sectioned dendritic black spheroidal particle (field ~50μ × 50μ): (a) microphotograph; (b) Ca K_α picture; (c) Fe K_α picture; (d) Si K_α picture; (e) Zr L_α picture; (f) Ti K_α picture; (g) Ba L_α picture; (h) S K_α picture 65

33. Photographs of a dendritic black spheroidal particle: (a) microphotograph; (b) Ca K_α particle; (c) Fe K_α particle; (d) Ca K_α particle (field ~50μ × 50μ); (e) Fe K_α particle (field ~50μ × 50μ); (f) Si K_α particle (field ~50μ × 50μ); (g) Ti K_α particle (field ~50μ × 50μ) 67

34. Leaching of radioiodine from powdered 1450°K eutectic $CaO-Al_2O_3-SiO_2$ doped with I^{131} 75

35. Leaching of radioiodine from powdered 1450°K eutectic $CaO-Al_2O_3-SiO_2$. The data have been fitted to the Elovich equation 76

TABLES

1. Compositions of Silicates used in Diffusion Studies 16

2. Diffusion Coefficients for Transport of Radionucles in Silicates 19

3. Thermodynamics of Formation of Gaseous Alkali Metal Oxides from Gaseous Elements 40

4. Description of Black Fallout Particles Subjected to Microprobe Analysis 69

5. Coefficients for the Elovich Equation at 300°K 74

6. Composite Cs^{137} Profiles in Three Johnie Boy Particles 78

CLOUD CHEMISTRY OF FALLOUT FORMATION

FINAL REPORT

by

J. H. Norman and P. Winchell

General Atomic Report GA-7597

SUMMARY

A transpiration method was used to measure Henry's law constants as a function of temperature for cesium and rubidium dissolved in eutectic $CaO-Al_2O_3-SiO_2$. Diffusivities of cesium, rubidium, potassium, sodium, indium, tin, and iodine in this matrix and other matrices were determined with either a vaporization method or a plane source-sectioning method.

Results of calculations obtained by using a Henry's-law-constant absorption, condensed state diffusion-controlled calculational model for fission product distribution in fallout are presented. This scheme leads to the conclusion that fission product fractionation is mainly a property of the fallout particle size distribution and the particle sizes under consideration. Also, deviations of these calculations from the Miller-model type of calculation are considered.

The stabilities of the alkali metal oxides as determined by Knudsen cell-mass spectrometric techniques are reported. The species $Cs_2O(g)$ and $Cs_2O_2(g)$, in particular, exhibit a much higher degree of stability than has been supposed.

Electron microprobe studies of particles from a seeded Eniwetok detonation are described. Thermal and chemical histories of some particles are traced through dendritic forms, accretion events, occurrence of the seeding elements, etc.

Results of some leaching studies, as they pertain to the condensed state diffusion-controlled, fission product absorption model, are presented.

INTRODUCTION

Studies of cloud chemistry and its effects, conducted at General Atomic during the past two years, have been concentrated primarily in seven areas:

1. Measuring high temperature equilibria between fission product elements in an oxidizing atmosphere and molten silicates.
2. Measuring diffusivities of these fission product elements in these silicates.
3. Measuring thermodynamic properties of gas phase species.
4. Integrating data and concepts into a mathematical description of the phenomenology important in describing the distribution of fission products in fallout.
5. Investigating the distribution of fission products in fallout.
6. Investigating the biological availability of fission products from fallout.
7. Considering other cloud chemistry phenomena, their importance, and how they might affect the constructed mathematical description.

These studies have led to a better qualitative and quantitative understanding of the fractionation of fission products during fallout formation and its effects.

STUDIES OF HENRY'S LAW CONSTANTS

INTRODUCTION

Previous efforts to determine Henry's law constants for cesium in silicates have been described in earlier reports.[1,2,3] Because of kinetic difficulties and other experimental problems encountered in these previous studies, an effort has been made to perform transpiration studies under more favorable conditions than were used before. The earlier transpiration studies were made at flow rates between 5 and 200 cc O_2/min, where diffusion effects were believed to be rate-limiting. That is, at gas flow rates of less than 5 cc/min, diffusion through the capillary was masking vapor pressure measurements, and at rates greater than 5 cc/min, condensed state diffusion was believed to be limiting cesium availability. For the present studies, two improvements were made in the transpiration system. The first improvement was to greatly reduce the diameter of the capillary so that the rate of diffusional transport of cesium through the capillary was lowered by about a factor of ten. The second improvement was to develop a method of data analysis which allows vapor pressure measurements to be made in the presence of considerable diffusional flow.

In order to understand the new method, it is necessary to consider the diffusional flow-vapor pressure coupling. Merten[4] has presented an analysis of the slug flow-diffusional flow problem for transpiration studies. The result he obtains by assuming that the vapor flow k (mass transport rate in the vapor) through a transpiration capillary of length λ and cross-sectional area A can be described by

$$k = A\left(Vc - D\frac{dc}{dx}\right) , \qquad (1)$$

STUDIES OF HENRY'S LAW CONSTANTS

INTRODUCTION

Previous efforts to determine Henry's law constants for cesium in silicates have been described in earlier reports.[1, 2, 3] Because of kinetic difficulties and other experimental problems encountered in these previous studies, an effort has been made to perform transpiration studies under more favorable conditions than were used before. The earlier transpiration studies were made at flow rates between 5 and 200 cc O_2/min, where diffusion effects were believed to be rate-limiting. That is, at gas flow rates of less than 5 cc/min, diffusion through the capillary was masking vapor pressure measurements, and at rates greater than 5 cc/min, condensed state diffusion was believed to be limiting cesium availability. For the present studies, two improvements were made in the transpiration system. The first improvement was to greatly reduce the diameter of the capillary so that the rate of diffusional transport of cesium through the capillary was lowered by about a factor of ten. The second improvement was to develop a method of data analysis which allows vapor pressure measurements to be made in the presence of considerable diffusional flow.

In order to understand the new method, it is necessary to consider the diffusional flow-vapor pressure coupling. Merten[4] has presented an analysis of the slug flow-diffusional flow problem for transpiration studies. The result he obtains by assuming that the vapor flow k (mass transport rate in the vapor) through a transpiration capillary of length λ and cross-sectional area A can be described by

$$k = A\left(Vc - D\frac{dc}{dx}\right), \qquad (1)$$

where V is the linear gas velocity, c is the vapor density at any point x in the capillary, and D is the interdiffusion coefficient for the carrier gas and the vapor.

Equation (1) can be evaluated for the inlet and outlet capillary boundary conditions $x = \lambda$; $c = c_1$ and $x = 0$; $c = 0$, which leads to Merten's final equation

$$P = \frac{k\,RT}{vM}\left[1 - \exp\left(\frac{-v\lambda}{DA}\right)\right] , \qquad (2)$$

where P is the species pressure at $x = \lambda$, v is the flow rate through the capillary in volume units, R is the gas constant, T is the absolute temperature, and M is the molecular weight of the species. This equation can be reduced to a type of universal equation for the purpose of data-fitting:

$$K = \frac{\nu}{1 - e^{-\nu}} , \qquad (3)$$

where $K = k\lambda\, RT/DAMP$ and $\nu = \lambda v/DA$. A log-log plot of Eq. (3) is presented in Fig. 1. The value of this particular plot becomes apparent when one considers the asymptotes. As ν goes toward zero, K goes toward unity; and as ν goes toward infinity, K goes toward ν. To fit transpiration data to this equation, one has just to plot the logarithm of the rate of transpiration, k, versus the logarithm of the flow rate, v, and fit the experimental curve to the universal curve by simple axes translation. From this "best fit," one obtains the "best" experimental values of DA/λ and MP for the experimental temperature involved.

EXPERIMENTAL STUDIES OF CESIUM AND RUBIDIUM

The type of data analysis described above has been used to study the vaporization of cesium and rubidium from the 1450°C eutectic CaO-Al_2O_3-SiO_2 as a function of temperature at flow rates between 0.01 and 8 cc/min of carrier gas. The carrier gas composition was varied from oxygen to argon, to air, and to water-saturated oxygen.

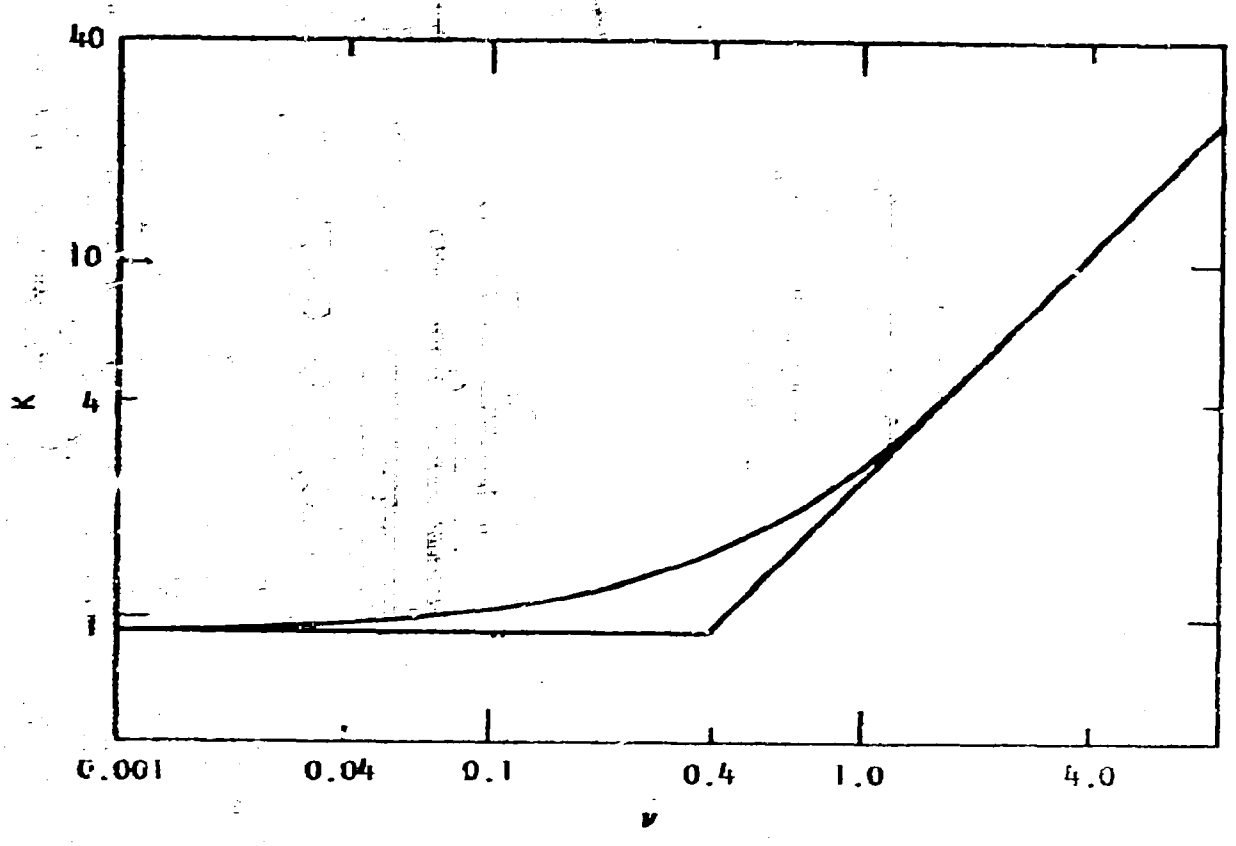

Fig. 1. Universal curve for transpiration studies with gaseous diffusion in the capillary

The experiments were performed with the transpiration apparatus shown in Fig. 2. A sample of the eutectic silicate loaded with either radiocesium or radiorubidium was placed in the bottom of the transpiration tube. The capillary tube was inserted in the sample-containing tube, and the system was then installed in a platinum resistance furnace. The temperature of this temperature-regulated furnace was measured by a series of thermocouples which had been calibrated against a standard thermocouple probe placed in a tube similar to the transpiration apparatus and similarly located in the furnace. Actual sample temperatures were then measured with the calibrated thermocouples. During an experiment, the carrier gas was passed between the capillary tube and the sample tube and into the sample region. After becoming saturated with cesium or rubidium, the gas passed up the capillary. At the end of the capillary, a mullite tube very effectively removed the alkali metal vapor species from the carrier gas. After this tube was detached from the experimental apparatus, the amount of alkali metal that was transpired and caught on the mullite was determined by counting methods and related to the measured flow rate of gas and the specific activity of the alkali metal. For any subsequent experiment, a new mullite tube was installed to collect more alkali metal vapors.

Examples of flow rate data for cesium and rubidium are plotted in Figs. 3 and 4, respectively, with theoretical curves included for comparison. Vapor pressure data from the varied-temperature experiments are presented in Figs. 5 and 6 for cesium and rubidium in terms of Henry's law constants. The equilibrium heats measured for these two systems were 79 and 83 kcal/mole, respectively. These data appear to be reliable.

It is interesting to note that measured vapor pressures of rubidium did not exhibit a measurable dependence on carrier gas composition. This result, which can be seen in Figs. 4 and 6, appeared very controversial when it was first achieved. That is, it was believed that the alkali metals were dissolved in the silicate as a univalent ion and vaporized as the metal.

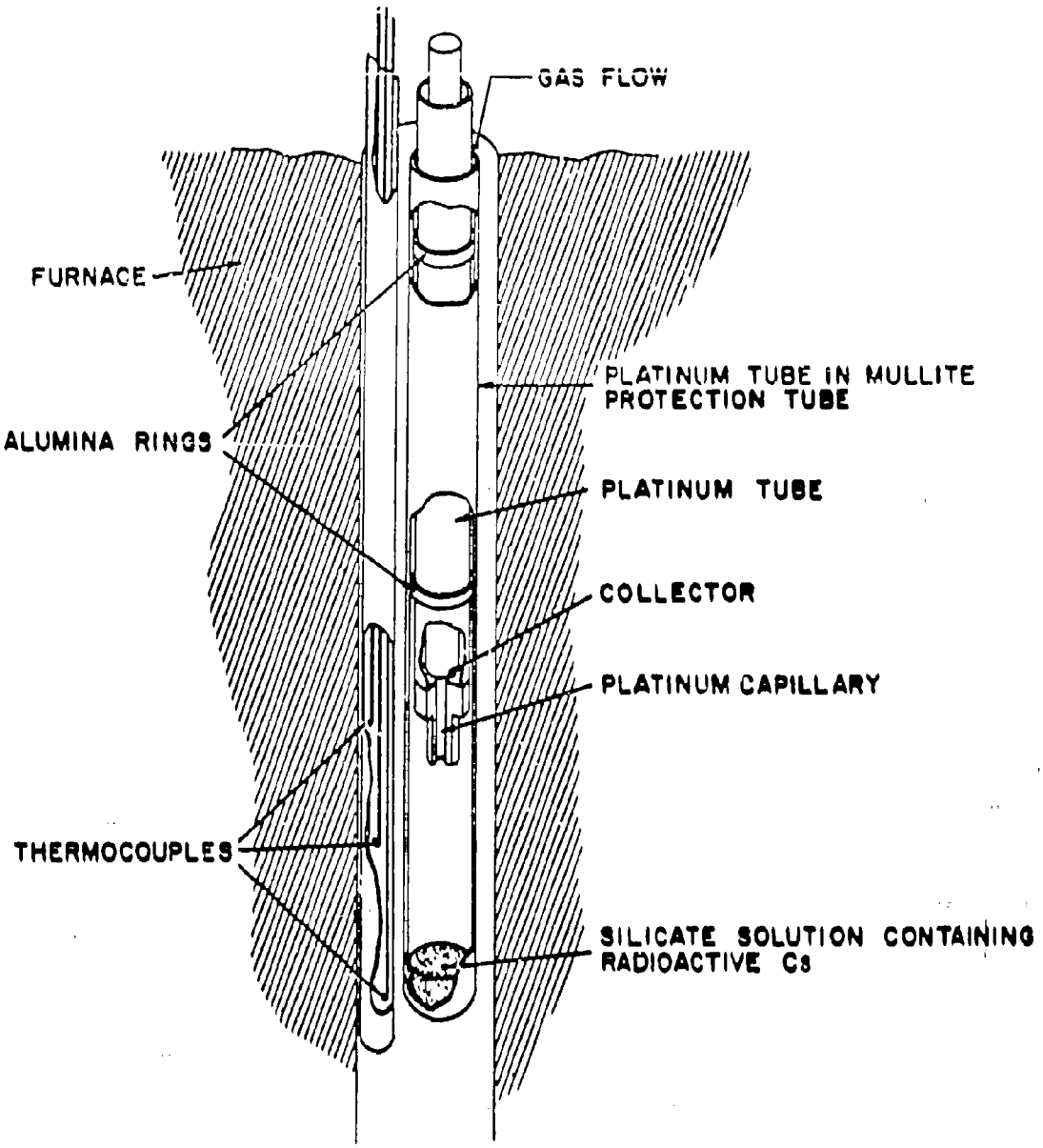

Fig. 2. Transpiration apparatus

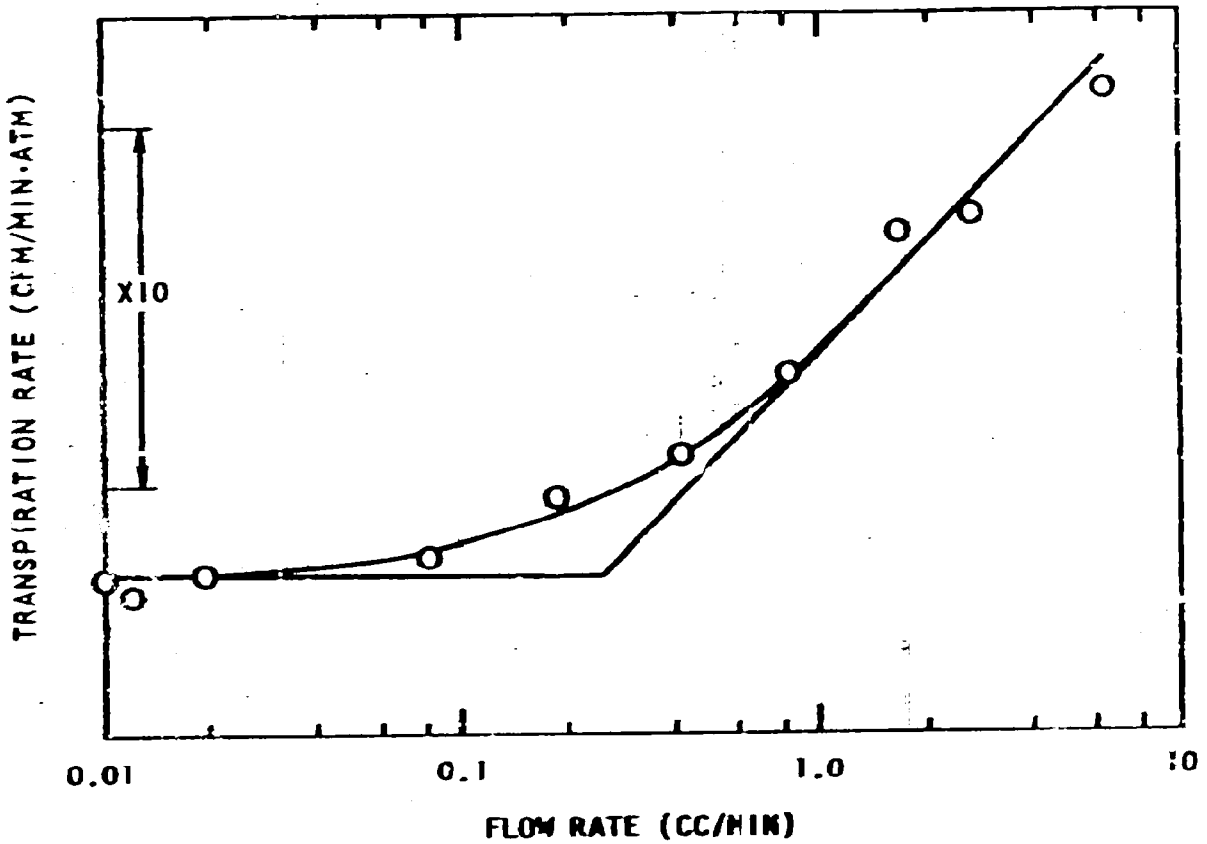

Fig. 3. Cesium transpiration from $CaO-Al_2O_3-SiO_2$ eutectic at 1785°K (P_{O_2} = 1 atm)

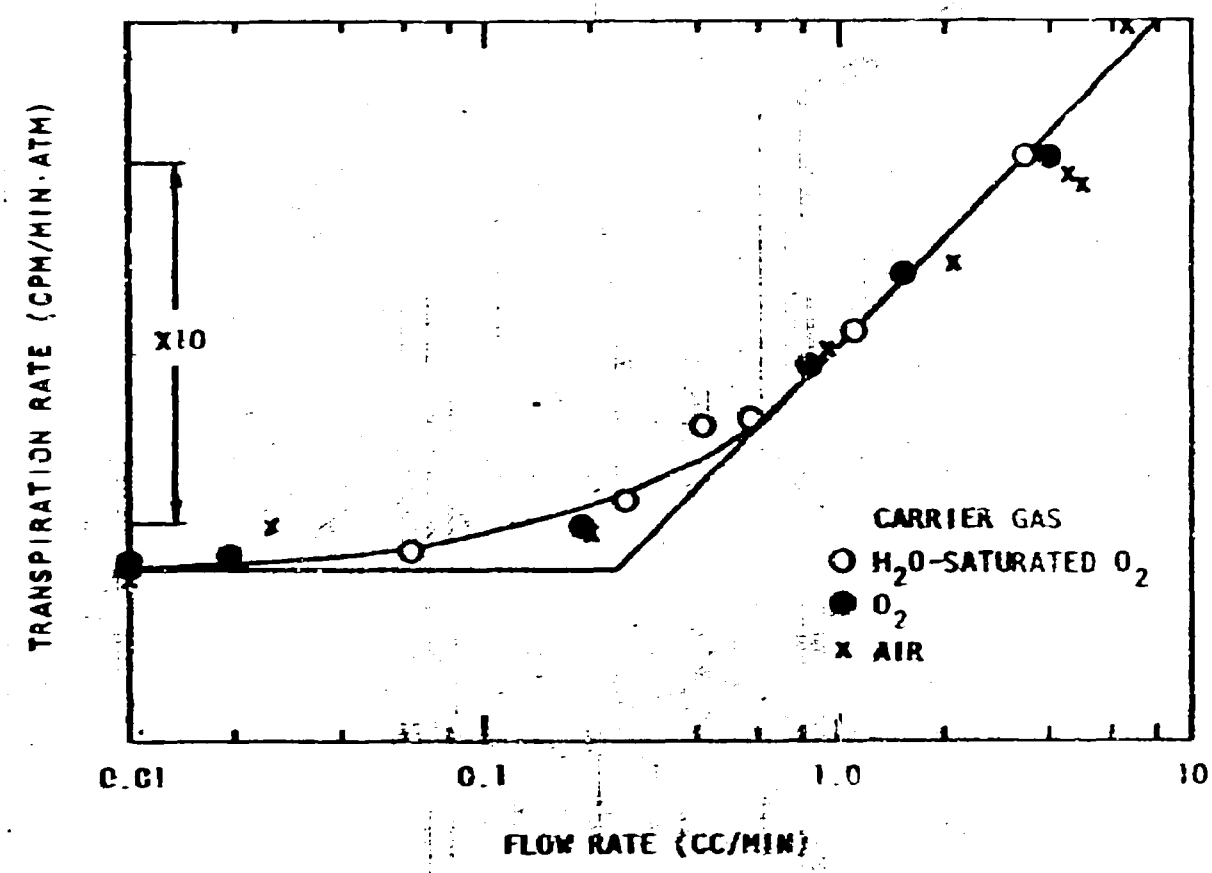

Fig. 4. Rubidium transpiration from $CaO-Al_2O_3-SiO_2$ eutectic at 1641°K (P_T = 1 atm)

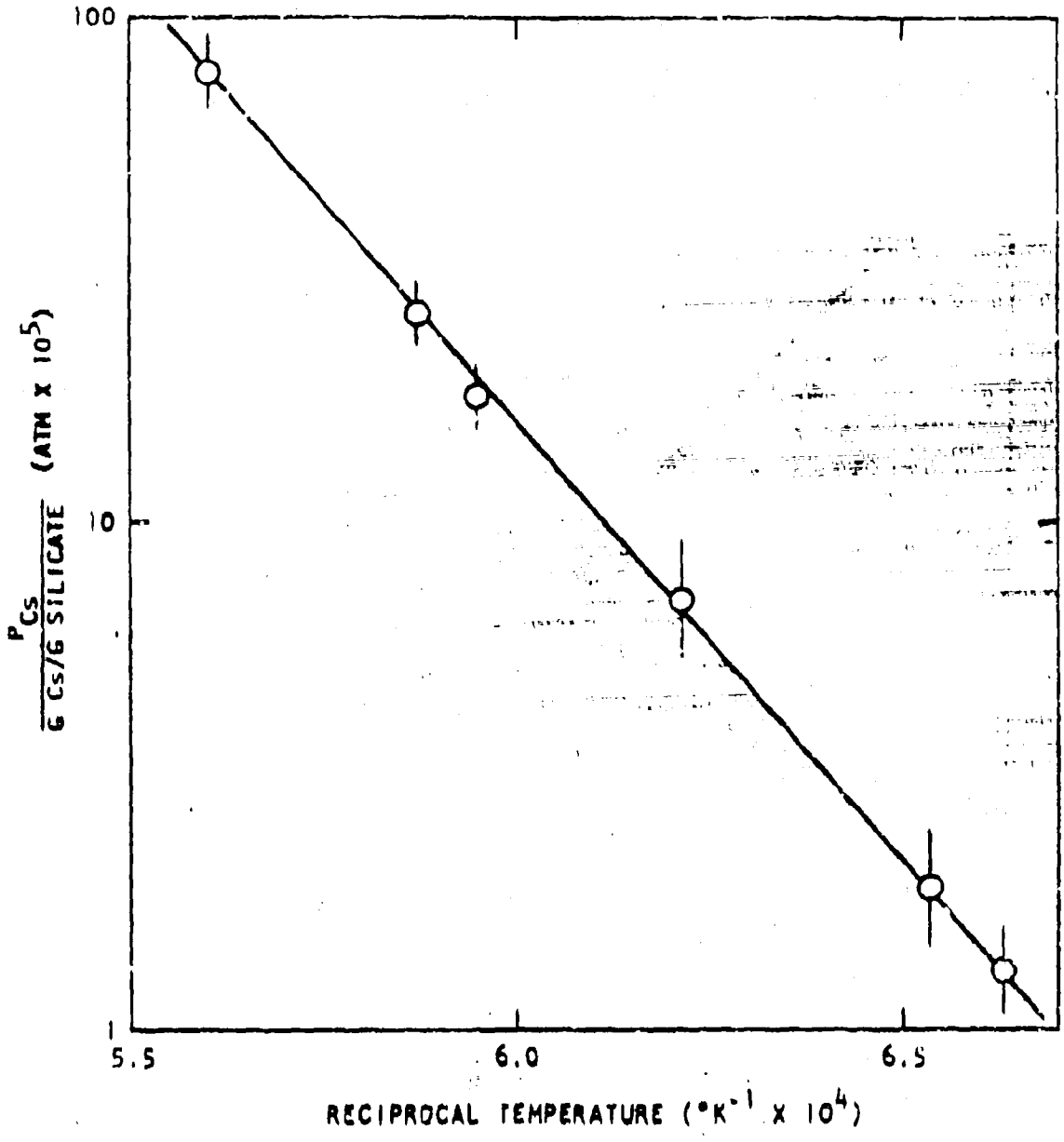

Fig. 5. Cesium vapor pressure per molten $CaO-Al_2O_3-SiO_2$ eutectic loading as a function of reciprocal temperature

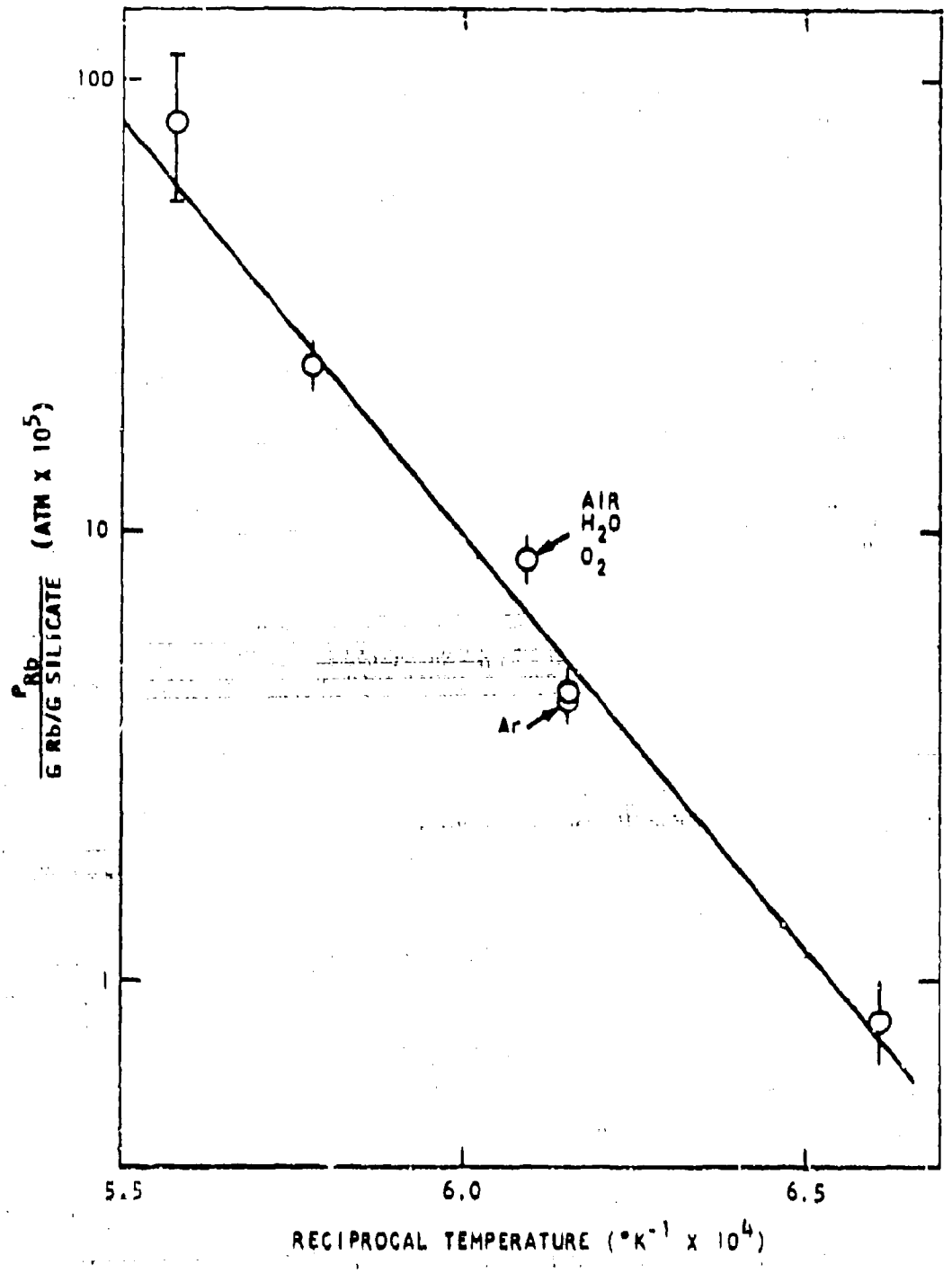

Fig. 6. Rubidium vapor pressure per molten $CaO-Al_2O_3-SiO_2$ eutectic loading as a function of reciprocal temperature

However, the present data support the concept of the vaporization of a compound in which the alkali metal is univalent but is not the hydroxide. Since the discovery of volatile alkali metal oxides and silicates, this result appears reasonable. The actual species transpired in these studies, however, remains unknown. Further studies may help reveal some more of the chemistry involved.

OTHER STUDIES

A study has been made to demonstrate the low absorption of iodine in a silicate from an oxidizing atmosphere. When iodine in O_2 was passed over eutectic $CaO\text{-}Al_2O_3\text{-}SiO_2$ at 1200°C, the sample was found to pick up 0.07 ppm iodine. Based on an estimated experimental iodine pressure, this sample has a Henry's law constant of 1.3×10^{-6} g iodine/g silicate-atm iodine at the experimental temperature. This value is even lower than that suggested in an earlier report on Henry's law constants in silicates[5] for the reaction

$$1/2\ SiO_2\ (sol) + I^- + 1/4\ O_2 \leftrightharpoons 1/2\ SiO_3^{=}\ (sol) + I(g)\ .$$

The experimental and calculated values indicate iodine to be so volatile during fallout formation that a more accurate value of the "Henry's law constant" would provide essentially no added information.

Indium transpiration studies have also been attempted. The volatility of this element appeared to be very low. In such cases, the actual value is unimportant in fallout. Transpired indium was not definitely identified in these studies. It was found, however, that platinum metal absorbed considerable indium from the 1300° to 1500°C glass even in an oxygen atmosphere. Indium studies have been abandoned.

The earlier report[5] on "Henry's law constants" in silicates includes values from the studies made at General Atomic and estimates for all important fission products and some activation products not studied. This report plus one on diffusivities[6] and another on the

condensed state, diffusion-controlled absorption model will provide information to aid in calculating the fate of various nuclides during fallout formation according to this model.

DIFFUSION OF RADIONUCLIDES IN MOLTEN SILICATES

INTRODUCTION

In Ref. 2, studies of diffusion in molten silicates were described. During the past two years, diffusion studies have been continued, with diffusion coefficients being obtained for the transport of iodine, rubidium, potassium, indium, tin, and sodium in the 1450°K eutectic of the $CaO-Al_2O_3-SiO_2$ ternary. Diffusion coefficients have also been obtained for transport of cesium in a $Na_2O-Al_2O_3-SiO_2$ matrix and in a matrix having the composition of reinforced concrete. Observation that the compensation law obtains for diffusion in silicates, combined with a correlation found between the coefficients in the diffusion equation and the reciprocal, effective ionic radius, has led to a method of estimating diffusivities in silicates with a minimum of experimental effort.

METHODS

The plane source technique and the vaporization technique, as described in Ref. 2, were used to obtain the data contained in the present report. For the rubidium, indium, and tin studies, radionuclides purchased from Oak Ridge National Laboratory (ORNL) were introduced into the silicate matrices at the 1% level. In studies involving cesium, potassium, and sodium, carrier nuclides were introduced into the silicate matrices at the 1% level and then activated by neutrons in the General Atomic TRIGA reactor to provide radioactive tracer isotopes. Attempts to directly introduce iodine into the matrices were unsuccessful. However, this problem was resolved by introducing enriched Te^{130} into the silicate and activating it in the ORNL research reactor to yield I^{131}. Three

DIFFUSION OF RADIONUCLIDES IN MOLTEN SILICATES

INTRODUCTION

In Ref. 2, studies of diffusion in molten silicates were described. During the past two years, diffusion studies have been continued, with diffusion coefficients being obtained for the transport of iodine, rubidium, potassium, indium, tin, and sodium in the 1450°K eutectic of the CaO-Al_2O_3-SiO_2 ternary. Diffusion coefficients have also been obtained for transport of cesium in a Na_2O-Al_2O_3-SiO_2 matrix and in a matrix having the composition of reinforced concrete. Observation that the compensation law obtains for diffusion in silicates, combined with a correlation found between the coefficients in the diffusion equation and the reciprocal, effective ionic radius, has led to a method of estimating diffusivities in silicates with a minimum of experimental effort.

METHODS

The plane source technique and the vaporization technique, as described in Ref. 2, were used to obtain the data contained in the present report. For the rubidium, indium, and tin studies, radionuclides purchased from Oak Ridge National Laboratory (ORNL) were introduced into the silicate matrices at the 1% level. In studies involving cesium, potassium, and sodium, carrier nuclides were introduced into the silicate matrices at the 1% level and then activated by neutrons in the General Atomic TRIGA reactor to provide radioactive tracer isotopes. Attempts to directly introduce iodine into the matrices were unsuccessful. However, this problem was resolved by introducing enriched Te^{130} into the silicate and activating it in the ORNL research reactor to yield I^{131}. Three

silicates have been used with some or all of these tracers. The compositions of these silicates are given in Table 1.

Table 1

COMPOSITIONS OF SILICATES USED IN DIFFUSION STUDIES
(In weight percent)

Component	Matrix		
	E[a]	RC	AQ[b]
SiO_2	62.0	48.0	74.0
Al_2O_3	14.7	13.0	4.0
CaC	23.3	10.5	
Na_2O		2.5	22.0
Fe_2O_3		10.8	
MgO		4.5	
K_2O		1.6	
Sb_2O_3		0.02	

[a] 1450°K eutectic.
[b] 1013°K eutectic.

All of these matrices were glassy in nature before and after the experiments except for the RC matrix that was used in the lowest-temperature experiment. Matrices E and AQ may be taken as representing geologically common soils. Matrix RC has a composition similar to that of reinforced concrete and certain basalts.

RESULTS

Examples of data obtained with the plane source technique and the vaporization technique are shown in Figs. 7 and 8, respectively. These data have been found to exhibit an Arrhenius dependence of the diffusion coefficient, D, which may be written as

$$\log D = A - BT^{-1}, \qquad (1)$$

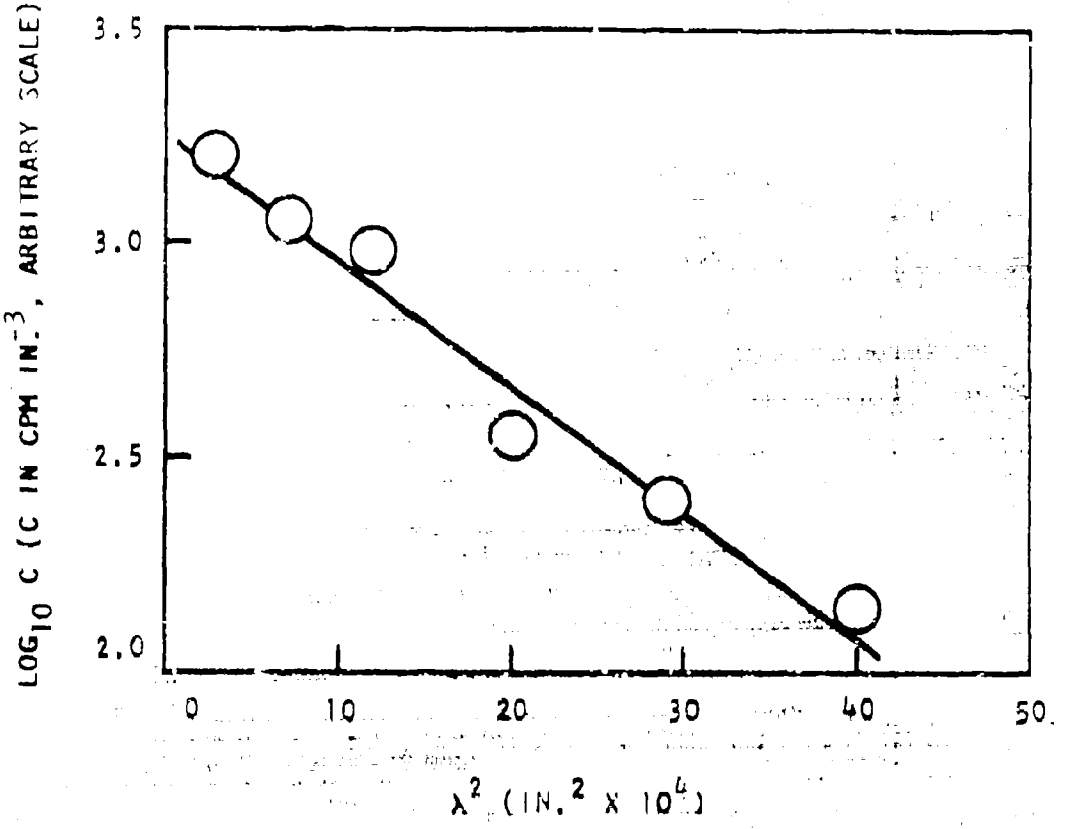

Fig. 7. Example of the penetration data from the plane-source technique for radiotin transport in the 1450°K eutectic of the $CaO-Al_2O_3-SiO_2$ ternary at 1°58°K. λ is the penetration distance.

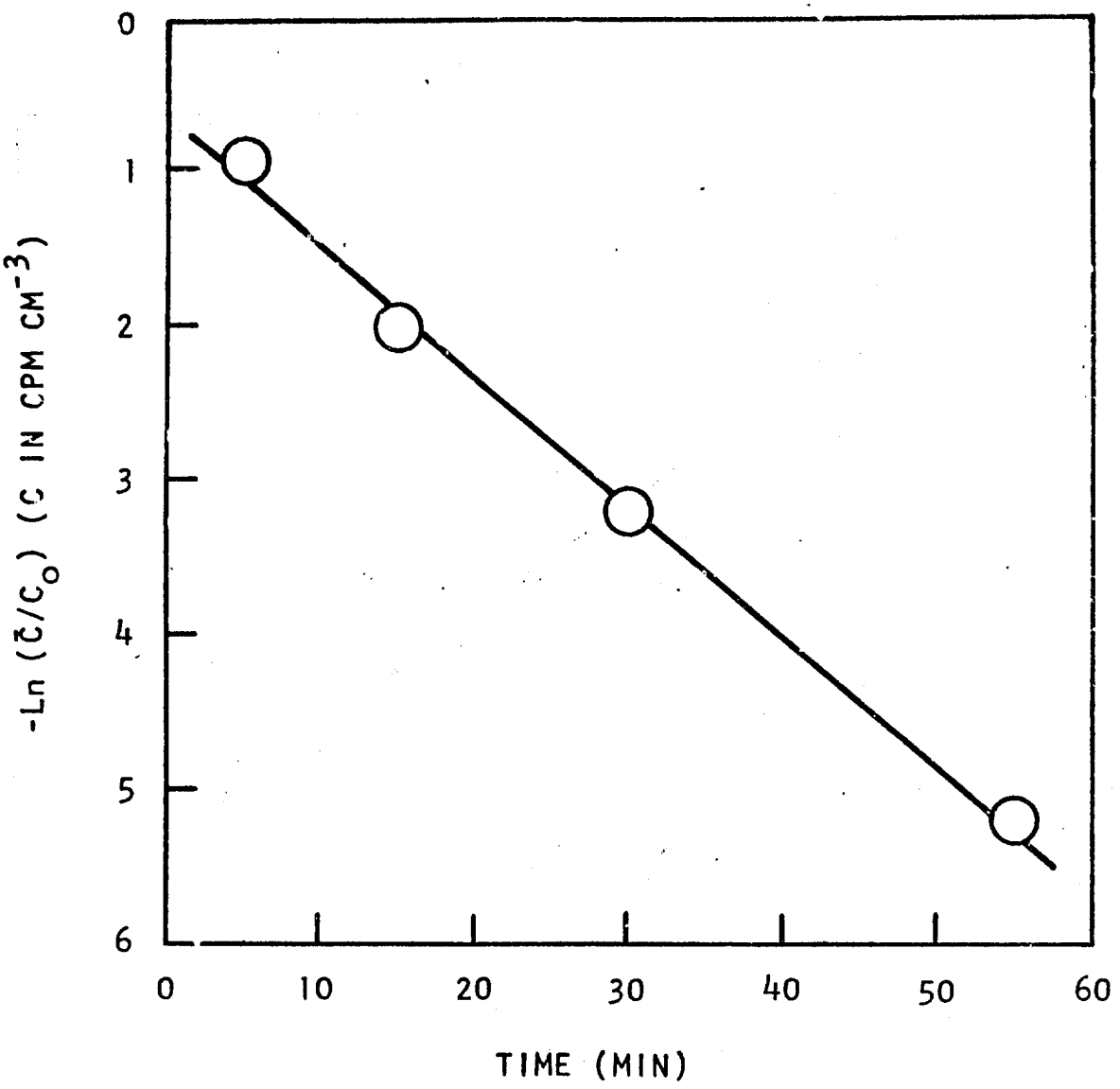

Fig. 8. Example of data from the vaporization technique for radio-rubidium transport in the 1450°K eutectic of the $CaO-Al_2O_2-SiO_2$ ternary at 1722°K

where D is in cm^2 sec^{-1} and T is in $^{\circ}K$. The coefficient B is related to the activation energy E^* by

$$E^* = 2.303\ RB\ , \qquad (2)$$

where E^* is in kcal $mole^{-1}$.

The results of these experiments are presented in Table 2 and in Figs. 9 through 16, where all of the data have been treated by the method of least squares with unit weighting. The uncertainties are ±50% for D and ±10°K for T. The uncertainty for D is not a standard deviation but includes, for example, compositional uncertainties.

Table 2

DIFFUSION COEFFICIENTS FOR TRANSPORT OF RADIONUCLIDES IN SILICATES

Species	Matrix	A	$B \times 10^{-3}$
I	E	7.29	22.5
Cs	RC	6.18	21.4
Rb	E	4.27	18.2
K	E	3.80	17.1
In	E	3.57	18.3
Sn	E	2.49	15.7
Na	E	0.14	10.0
Cs	AQ	-2.34	5.7

DISCUSSION

If one considers the values for A and B given in Table 2 and in a previous report on diffusion coefficients,[2] one finds that a striking linear correlation exists between these values. This correlation is shown in Fig. 17, where the least squares line drawn through the points was determined to be

$$A \pm 0.52 = -5.79 + 0.564\ B \times 10^{-3}\ , \qquad (3)$$

with B assumed to be measured exactly. The uncertainty that has been associated with A is the standard error of estimate[6a] which corresponds to an uncertainty of a factor of 3.3 for the diffusion coefficient, a remarkably small uncertainty.

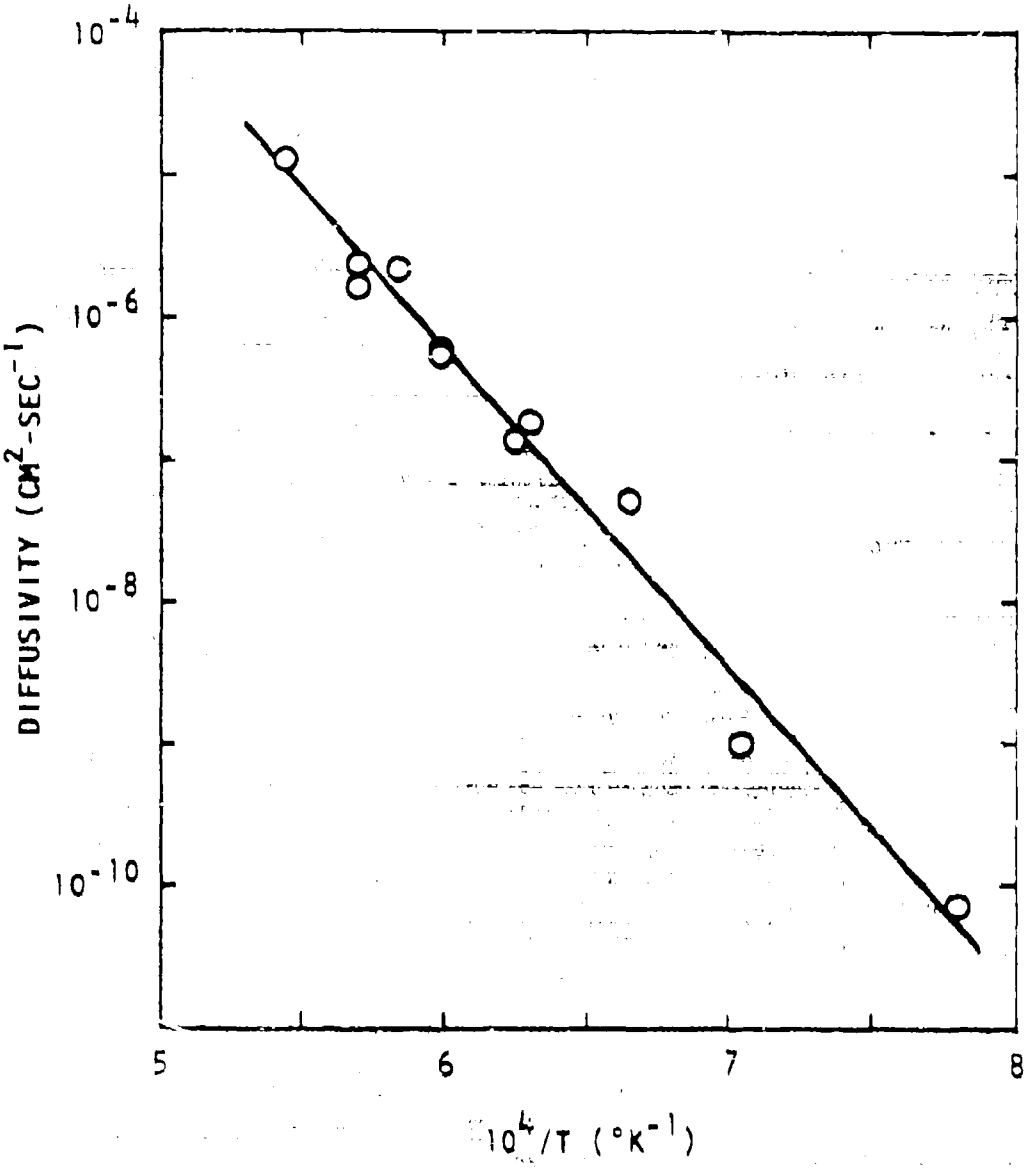

Fig. 9. Diffusivities for transport of radioiodine in 1450°K eutectic CaO-Al_2O_3-SiO_2 using the vaporization technique

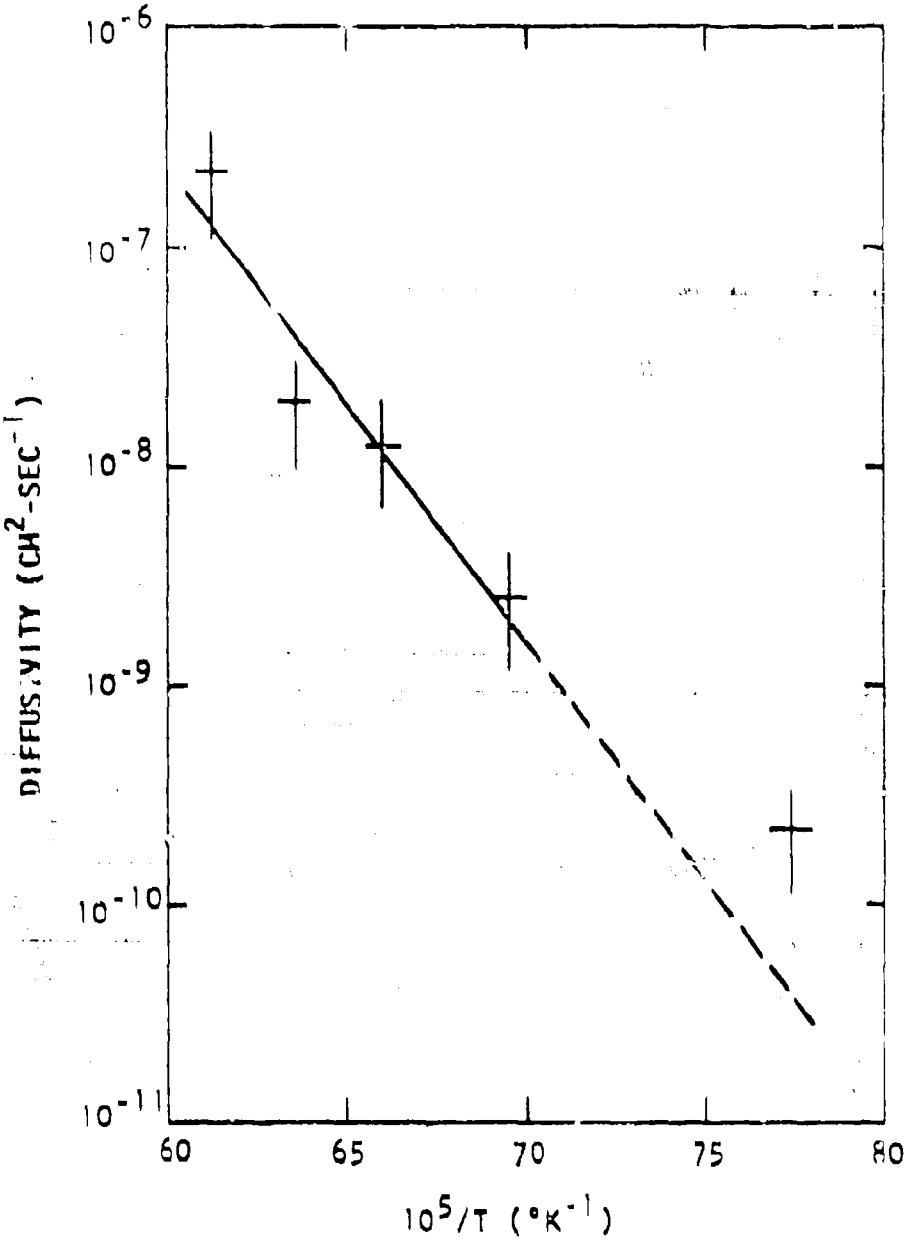

Fig. 10. Diffusion coefficients for transport of radiocesium in a molten CaO-MgO-Fe_2O_3-Al_2O_3-SiO_2 matrix using the plane-source technique. The low temperature sample was devitrified

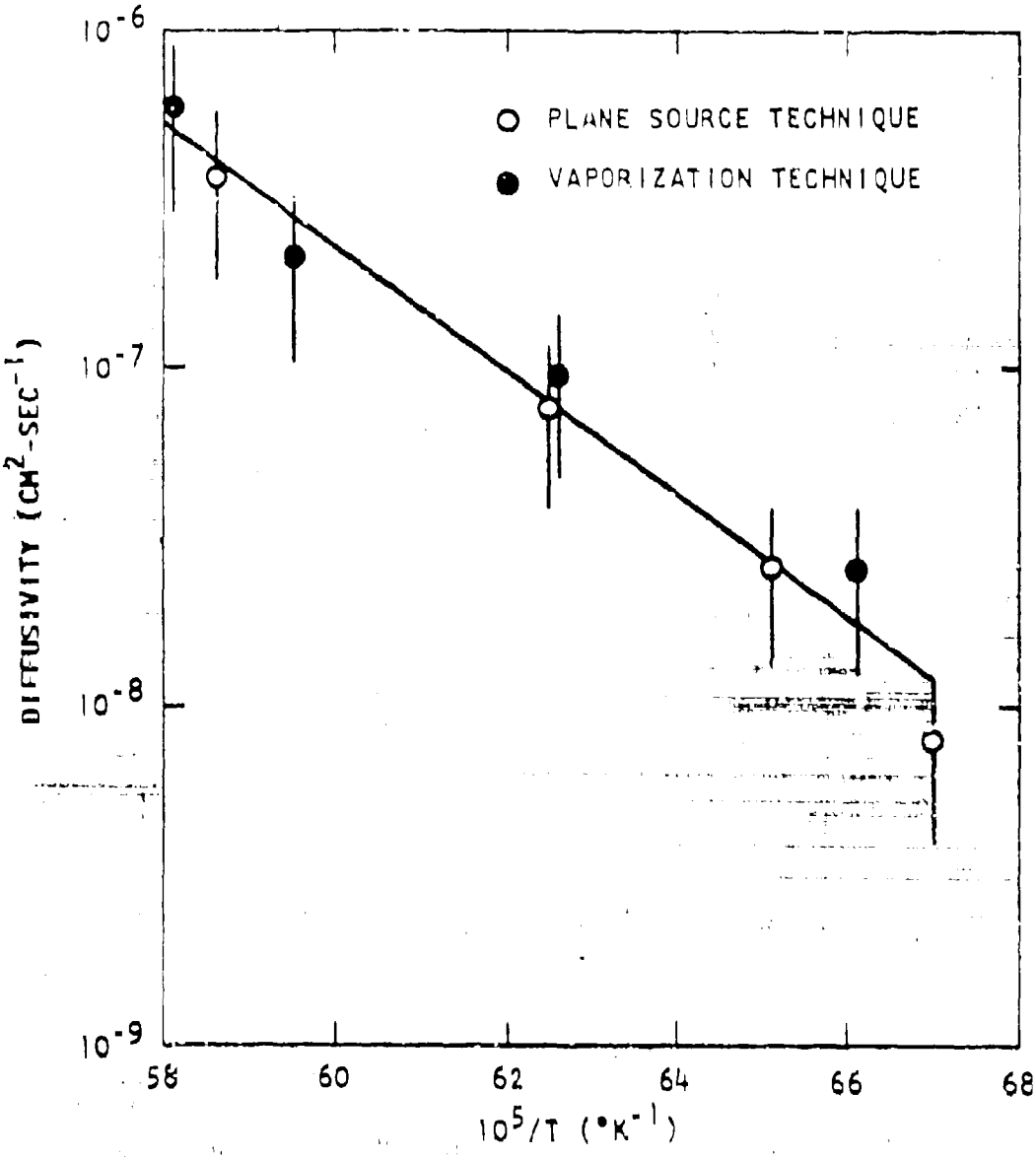

Fig. 11. Diffusion coefficients for transport of radiorubidium in molten eutectic $CaO-Al_2O_3-SiO_2$

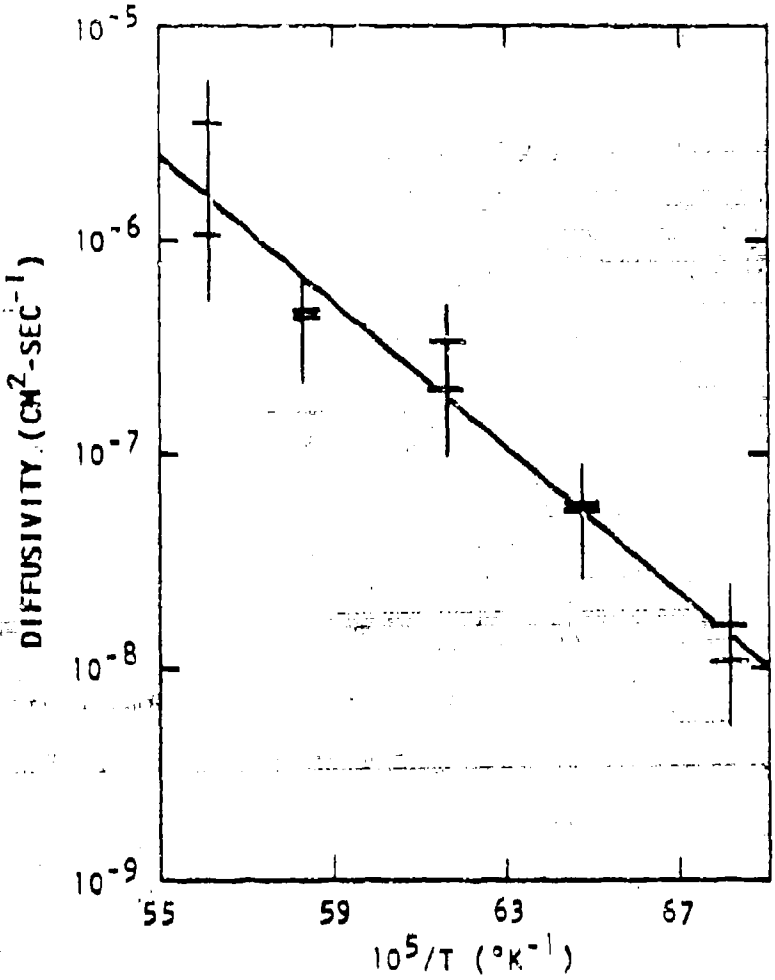

Fig. 12. Diffusion coefficients for transport of radiopotassium in molten eutectic CaO-Al_2O_3-SiO_2 using the plane-source technique

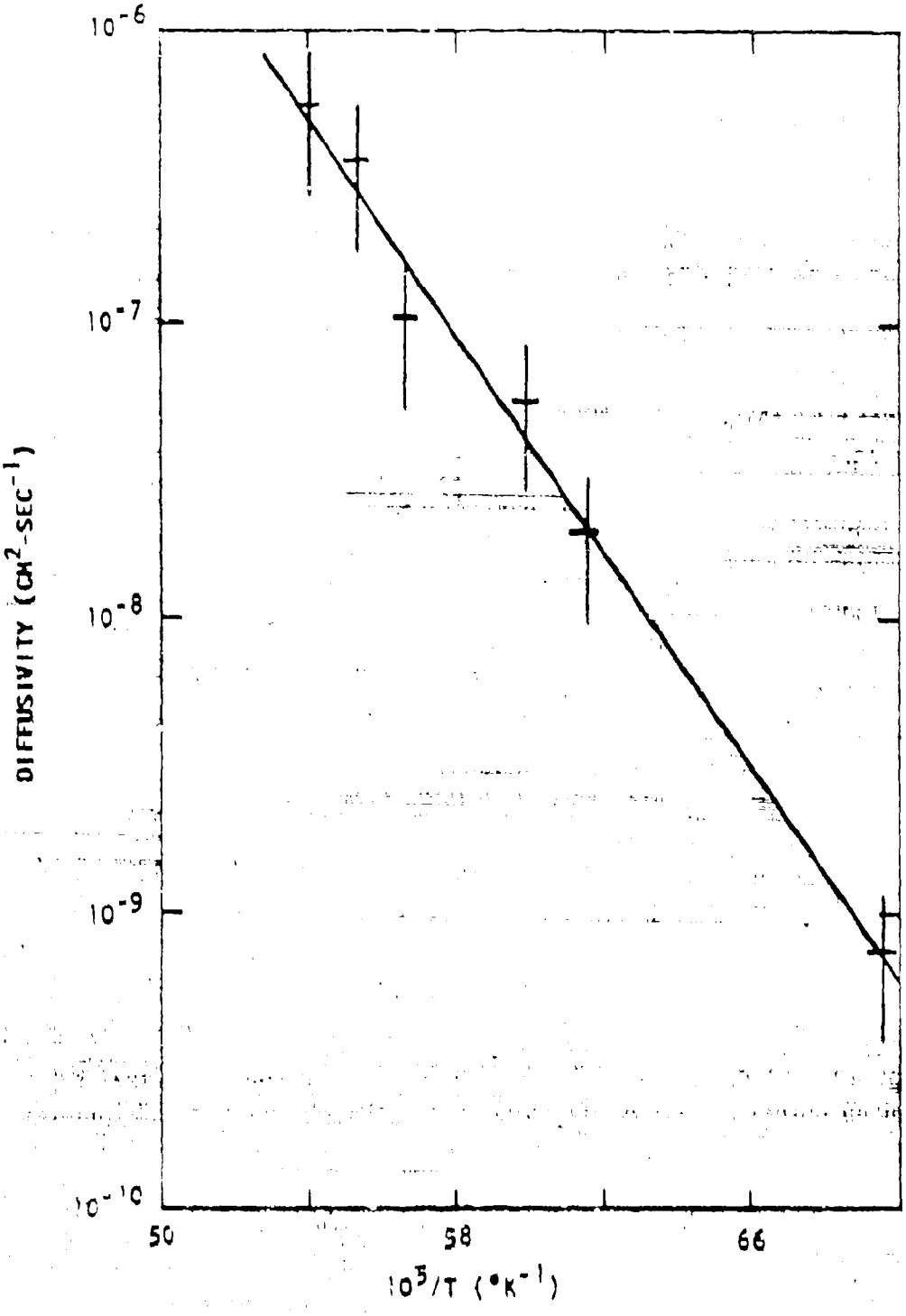

Fig. 13. Diffusion coefficients for transport of radioindium in molten eutectic CaO-Al_2O_3-SiO_2 using the plane-source technique

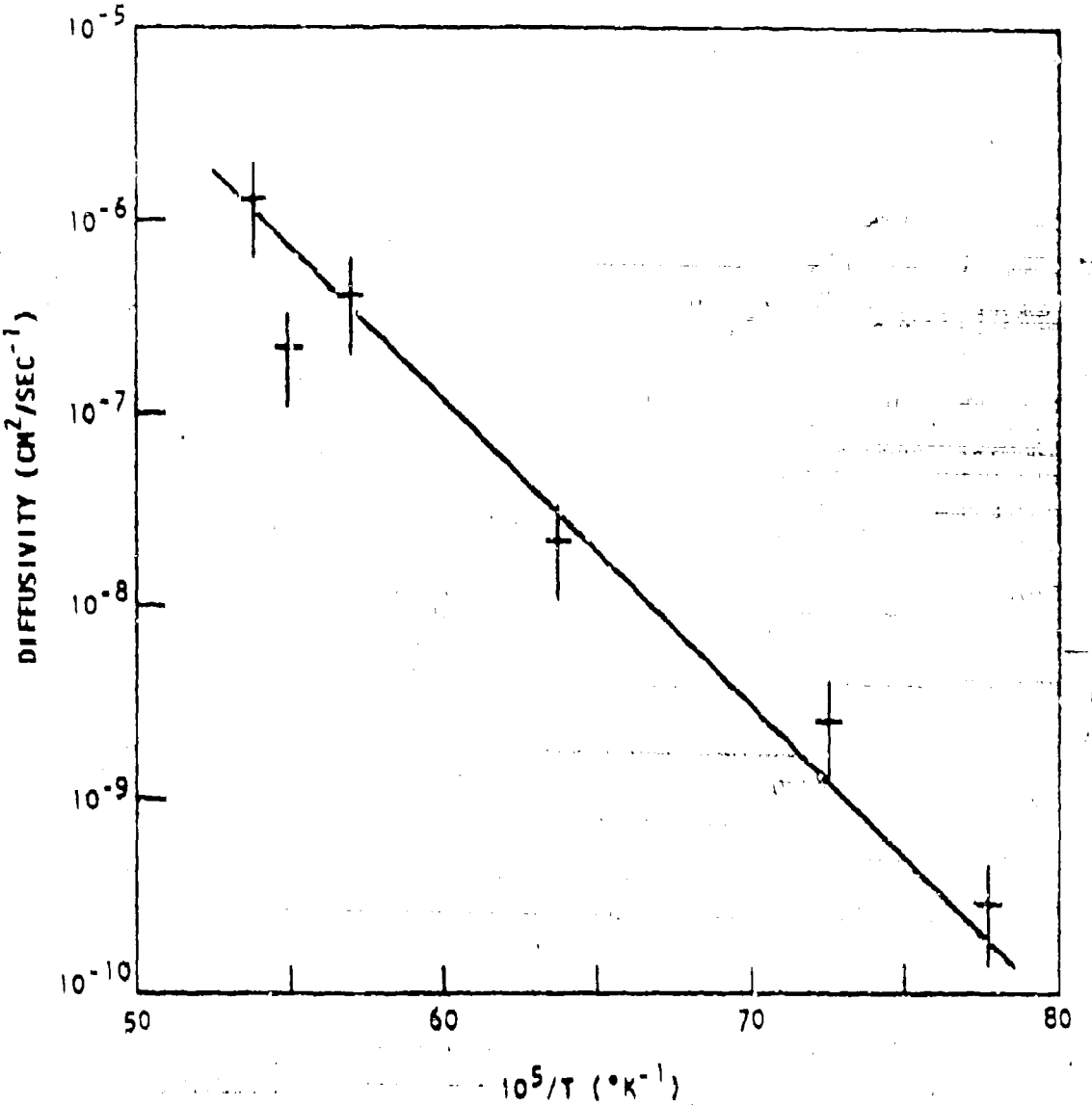

Fig. 14. Diffusion coeffients for transport of radiotin in molten eutectic $CaO-Al_2O_3-SiO_2$ using the plane-source technique

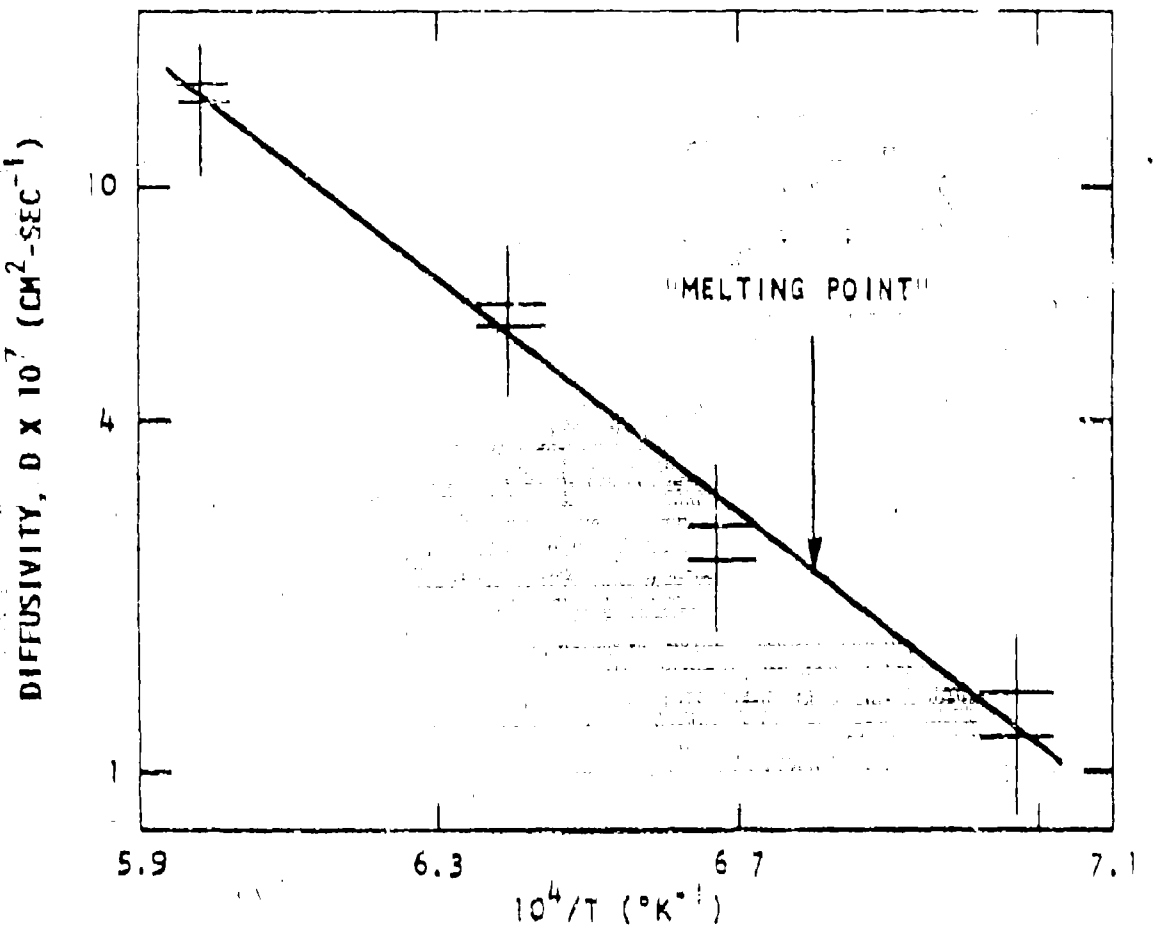

Fig. 15. Diffusion coefficients for transport of radiosodium in molten eutectic $CaO-Al_2O_3-SiO_2$ using the plane-source technique

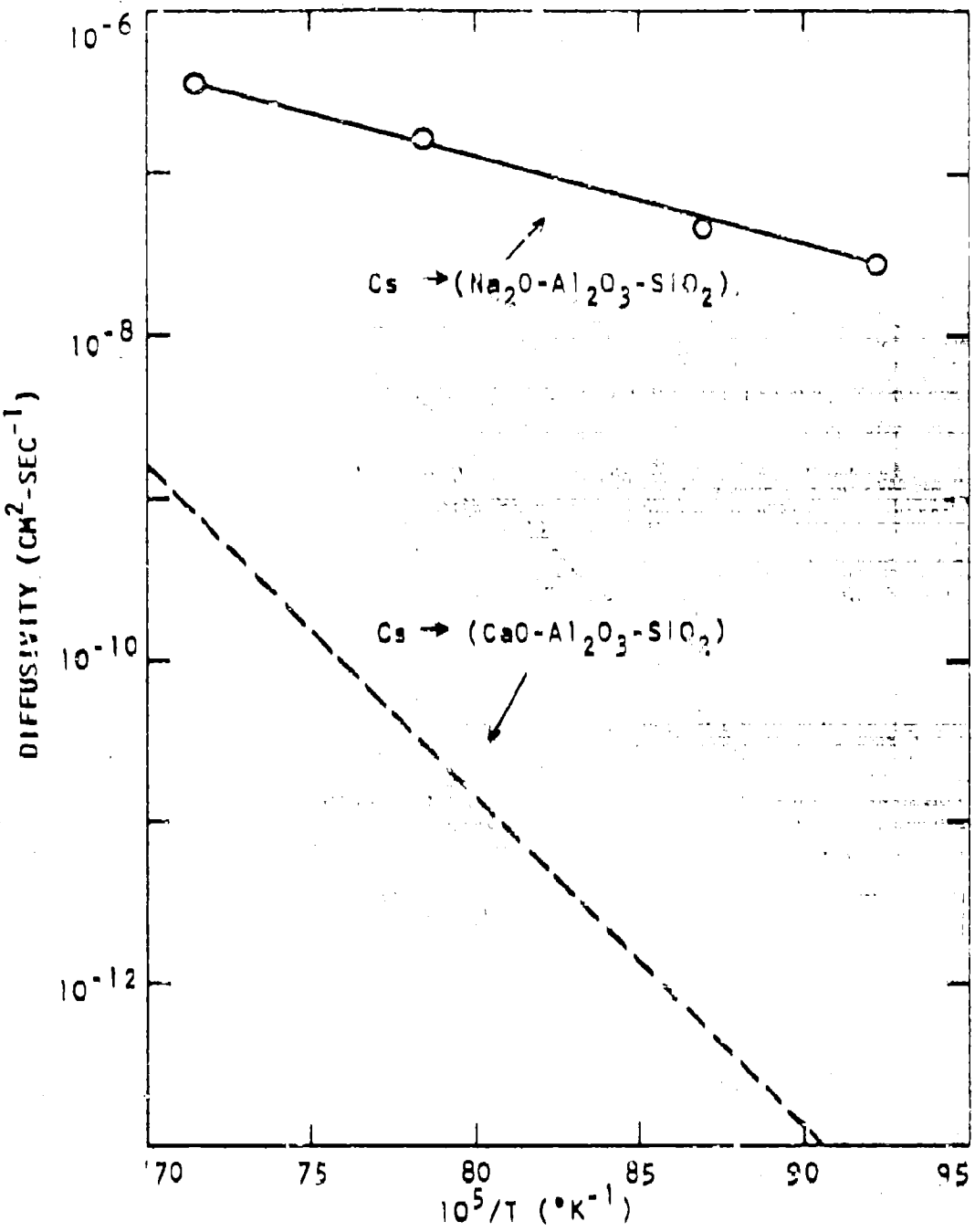

Fig. 16. Diffusion coefficients for transport of radiocesium in molten eutectic Na_2O-Al_2O_3-SiO_2. The dashed curve is an extrapolation of previously reported diffusivity in eutectic CaO-Al_2O_3-SiO_2

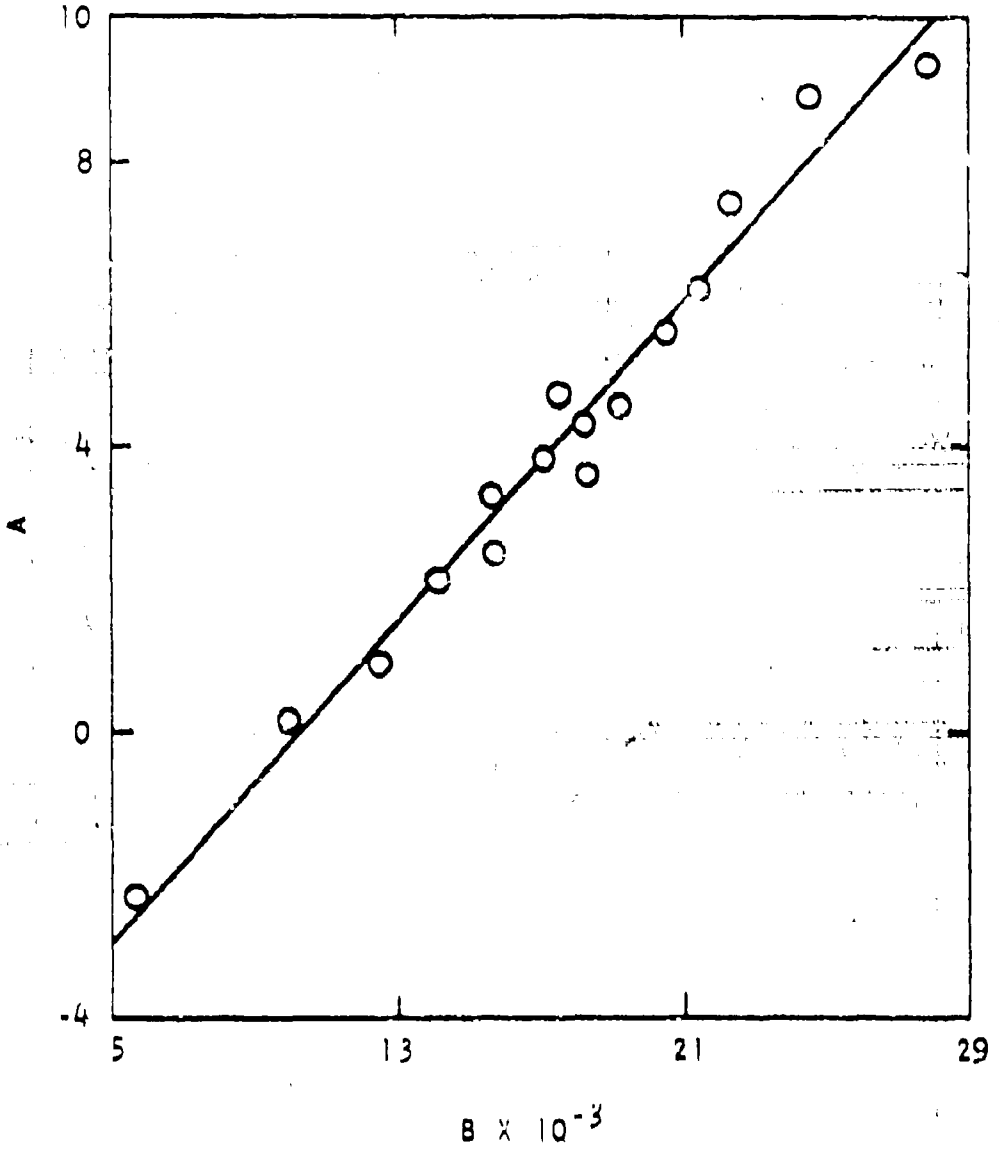

Fig. 17. A:B correlation for diffusion in molten silicates obtained in this laboratory

It is of interest to compare the results from this Laboratory with those reported by other laboratories. At General Atomic a set of more than 100 (A, B) points, including the 17 from the present studies, has been compiled. This collection, which is shown in Fig. 18, includes results of studies of the following nuclides diffusing in many different silicate matrices: magnesium, iodine, cesium, rubidium, potassium, sodium, lithium, indium, tellurium, tin, antimony, molybdenum, strontium, aluminum, calcium, phosphorus, sulphur, silicon, nickel, iron, vanadium, niobium, and silver. The matrices range from simple binary silicates to very complex ones exhibiting a wide range of chemical and physical properties. The approximate temperature range covered by the various studies was 300° to 2000°K. About 26% of the data are for diffusion of sodium in low melting binarys and ternarys. Because the sodium data are very similar and somewhat repetitious, they have been grouped and are represented in the calculations and in Fig. 18 as four points. A least squares treatment of all the diffusion data yielded

$$B \times 10^{-3} \approx 6 = 9.4 + 1.58 A \qquad (4)$$

The standard error of estimate corresponds to an uncertainty for the diffusion coefficient of a factor of 34 at 1700°K, which seems excessive. However, considering that the data were reported by many laboratories throughout the world, that several experimental techniques were used, and that very diverse systems are correlated here, the overall A:B correlation is surprisingly good. It is noted that certain subsets of the data exhibit A:B correlations which have less scatter than has the entire collection.

The importance of the A:B correlation to the fallout problem lies in its potential value as a tool for predicting diffusion coefficients. The need for a means of predicting diffusion coefficients becomes obvious when the effort involved in a purely experimental program for determining diffusion coefficients for the large array of soils and nuclides of interest in fallout formation is considered. Thus, with the use of the A:B

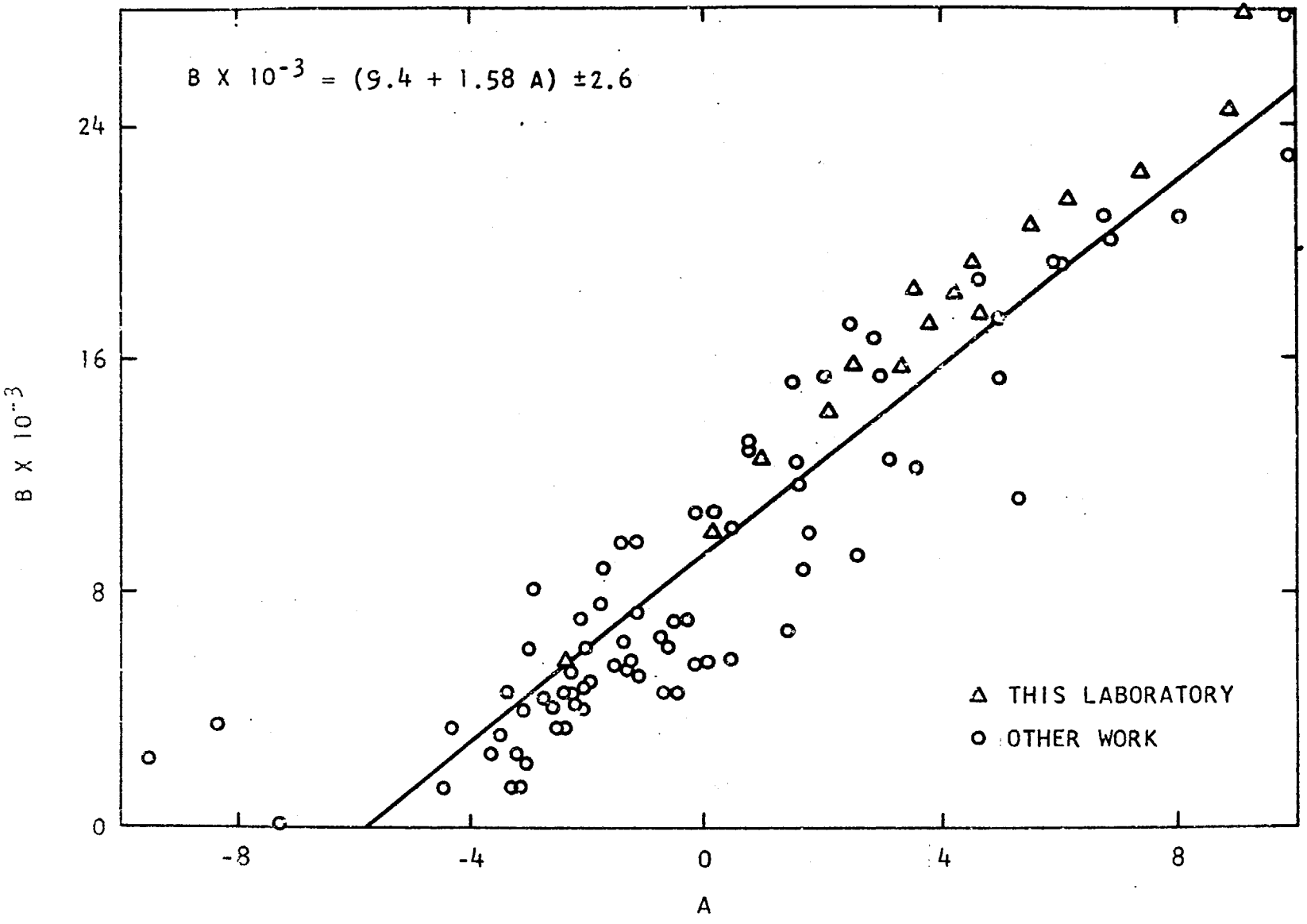

Fig. 18. Correlation between the coefficients in the diffusion equation, log D = A - BT^{-1}, for diffusion of nuclides in silicates

correlation, if a value of A (or B) can be obtained independently of B (or A), a diffusion coefficient can be predicted for transport of a particular nuclide in a particular matrix. It should be emphasized, however, that although the A:B correlation seems reasonably matrix-independent, individual values of A (and B) are strongly dependent upon composition. One secondary result of the overall A:B correlation is worth noting. From Eqs. (1) and (4), one finds that, for the present studies only and within the uncertainty of the correlation, all nuclides should have a diffusion coefficient of $\sim 10^{-7}$ cm^2 sec^{-1} at $\sim 1580^{\circ}$K or a slightly higher temperature. It is felt that this is not a trivial result but is associated with the nature of the system.

Evidently, the A:B correlation found for silicates is only a special case of what is called the compensation law or compensation effect. Another example of this phenomenon in chemical diffusion is found for diffusion in metallic copper[7] (see Fig. 19). Other examples are to be found in many other types of kinetic processes. As Rüetschi points out,[8] the A:B correlation has been observed for kinetics of homogeneous and heterogeneous reactions, for diffusion, viscosity, semiconductor conductivity, and electron emission. It has also been observed for dielectric relaxation in a variety of glassy materials.[9] Rüetschi[8] has published a theoretical treatment of the compensation law. He has shown that if the potential energy dependence on interatomic distance is anharmonic (e.g., exponential), and if this dependence does not vary greatly for a set of similar processes, a correspondence between A and B should be observed. More simply, within a series of compensated reactions there is a direct relationship between force constants of a vibrational system which is governing the diffusion (in this case) process and the bond energies associated with this system.

With the ability to obtain A from B or vice versa established, the establishment of either B or A remains. Some progress toward simplifying this problem empirically has been made. An empirical approach to the

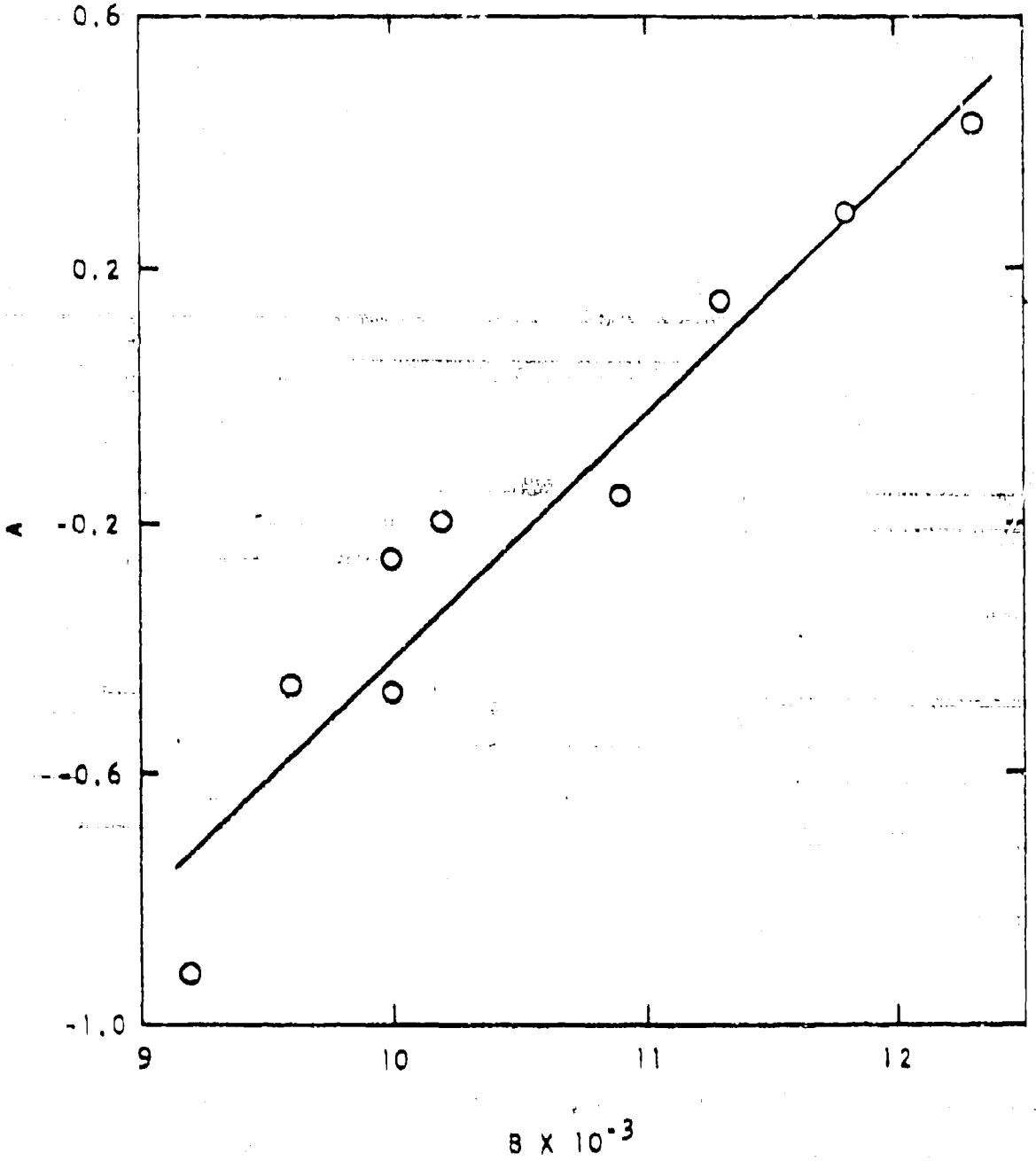

Fig. 19. Example of the compensation law. Diffusion of various metals in copper. Data taken from Ref. 8

problem of prediction was employed because there appears to be only very limited theory available with which to predict diffusivities in silicates. When the data for diffusion of cesium, rubidium, and sodium in matrix E from this Laboratory were considered, a linear correlation was observed between A (or B) and the reciprocal ionic radius, r^{-1}. The reciprocal ionic radius was chosen as a parameter because binding forces in minerals are often considered on the basis of the ionic potential Z/r, where Z is the formal charge of a cation and r is the corresponding ionic radius.[10] On the basis of the correlation for cesium, rubidium, and sodium, values of A and B were predicted for potassium before the experiments for potassium were initiated. The experimental values agreed reasonably with the predicted values, as is shown in Fig. 20. Also, it was later established that the value of A obtained for iodine fitted well in the $A:r^{-1}$ correlation for the four alkalies if I^{-1} was assumed to be the diffusing species. Thus, if this correlation holds in another system two measurements will suffice to estimate diffusivities of many elements.

It is necessary to include in any system the multiply charged species. Diffusion measurements have been made for indium, tellurium, tin, antimony, and molybdenum, but attempts to include them directly in an overall A:Z/r correlation were not successful. On the basis of the present limited data, an empirical effective ionic radius appears to allow representation of multiply charged species. Thus:

1. For singly charged species, the effective ionic radius, ρ, is identical to r. For halides, $r = \rho$ is that radius corresponding to the X^{-1} oxidation state.
2. For multiply charged species, the effective ionic radius is $\rho = 1.59\ r$, where r is that ionic radius corresponding to the most probable oxidation state in the silicate at high temperature.

This correlation for the present results with matrix E is shown in Fig. 21. In this figure, the line drawn through the points resulted from a least squares treatment of the data which gave

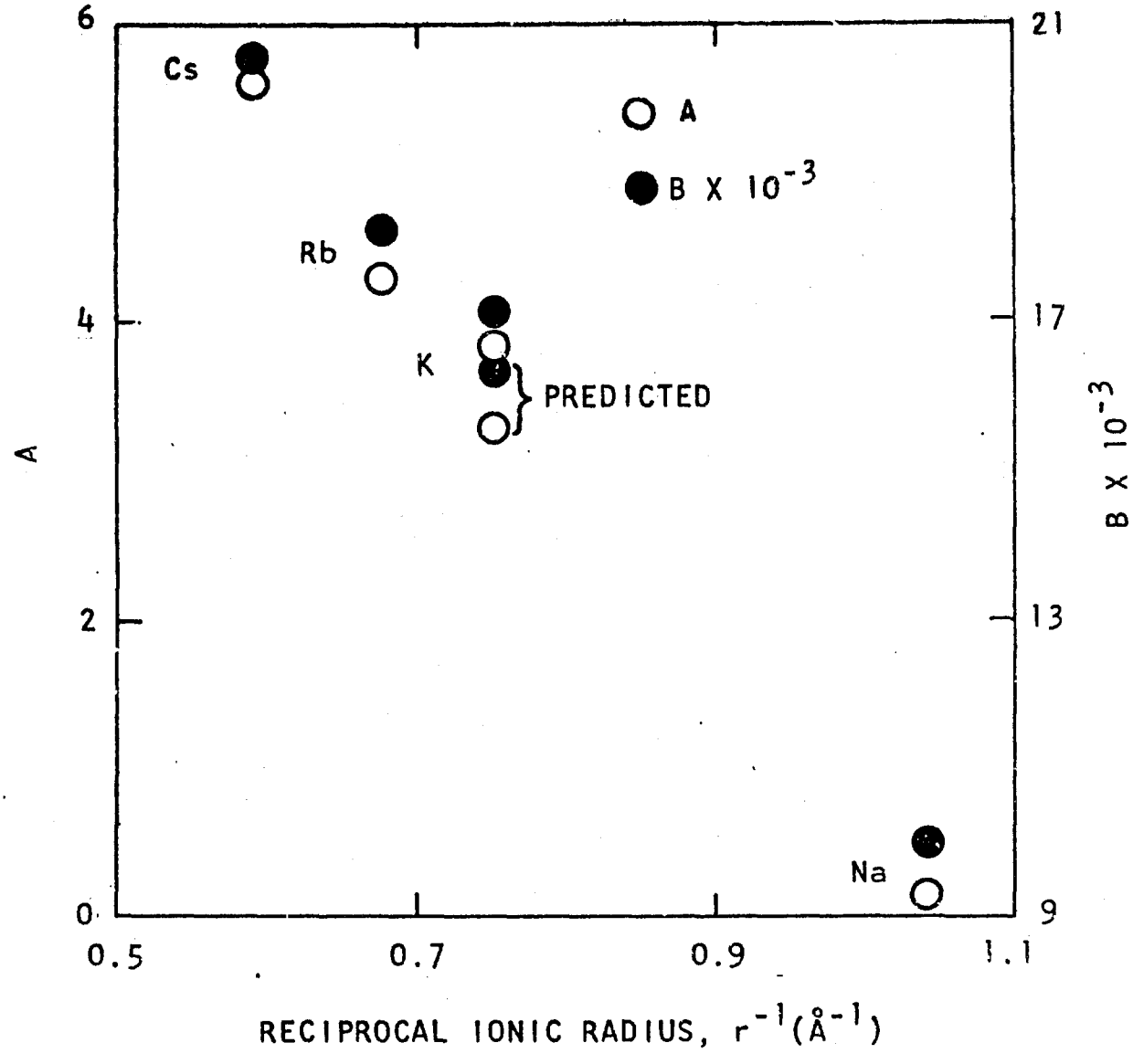

Fig. 20. Correlation of coefficients in the diffusion equation, $\log D = A - BT^{-1}$, with reciprocal ionic radius for diffusion of cesium, rubidium, potassium, and sodium in molten eutectic $CaO\text{-}Al_2O_3\text{-}SiO_2$

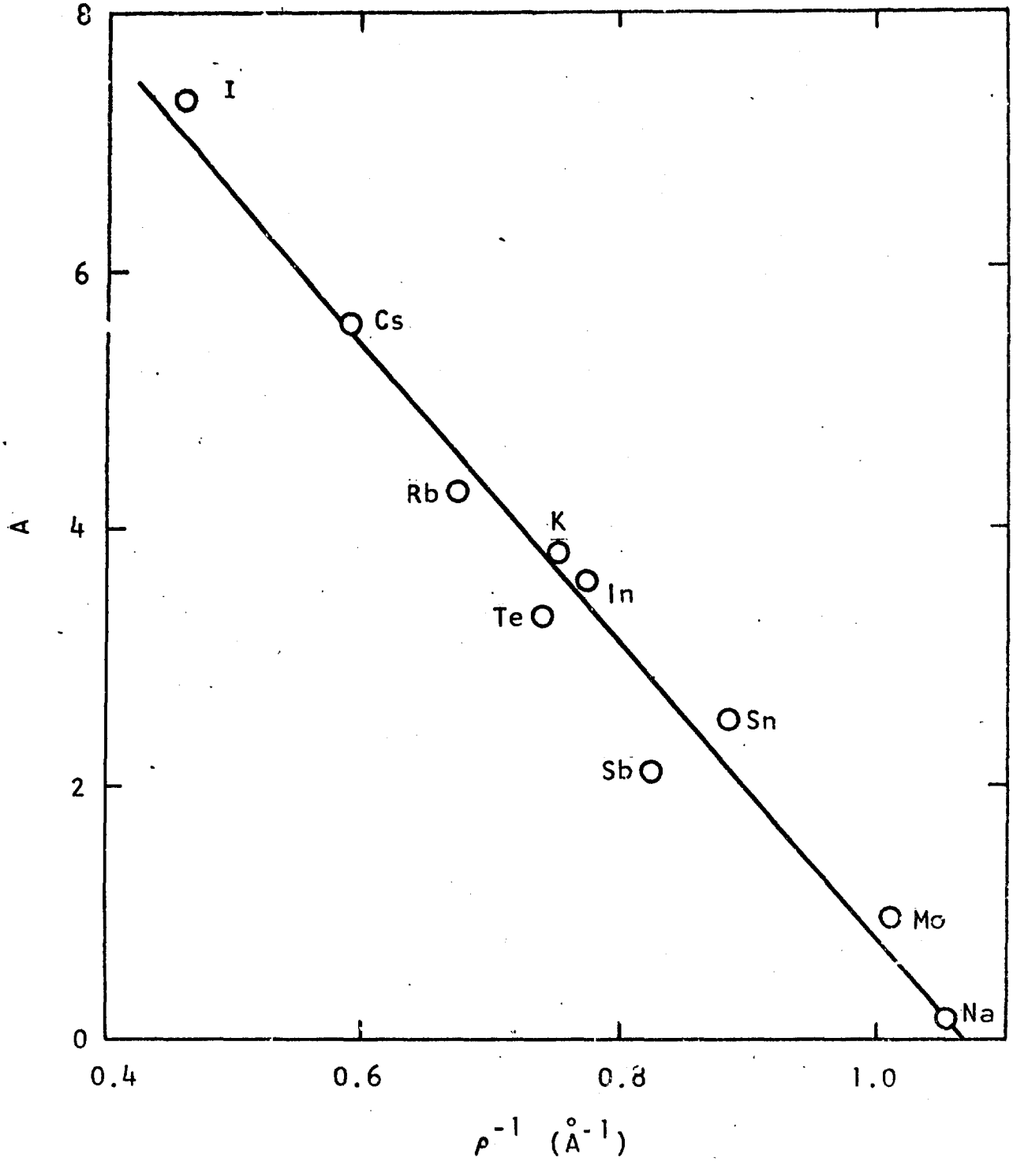

Fig. 21. Correlation between A in log D = A - BT^{-1} with reciprocal effective ionic radius for diffusion in the 1450°K eutectic of the CaO-Al_2O_3-SiO_2 ternary

$$A \pm 0.38 = 12.35 - 11.58\,\rho^{-1} \quad , \tag{5}$$

where the uncertainty is the standard error of estimate. Thus, from Eqs. (3) and (5), one obtains

$$(\log D) \pm 0.86 = 12.35 - 11.58\,\rho^{-1} - 32.16 \times 10^{3}\,T^{-1} + 20.53 \times 10^{3}\,\rho^{-1}T^{-1} \quad , \tag{6}$$

from which the diffusivity of some particular species in matrix E can be found. It is emphasized that Eq. (6) pertains only to the 1450°K eutectic of the $CaO\text{-}Al_2O_3\text{-}SiO_2$ ternary. The coefficients in Eq. (5) may change strongly if another matrix is considered.

If these A, B, ρ^{-1} correlations were to hold for another matrix, then only two diffusion measurements with two different species at $T \neq \sim 1600°K$ need be made with the new matrix in order to make diffusivity predictions for other species in this matrix. The value 1.59 as applied to polyvalent species alone is not scientifically pleasing, and it will be necessary to attempt to clarify the $A:\rho^{-1}$ correlation further.

The $A:\rho^{-1}$ correlation found in this Laboratory can be tested somewhat. Ralkova[11] has reported diffusivities for transport of strontium, cesium, potassium, sodium, and lithium in a low melting silicate; for the four alkalies at one temperature, her data are given as a linear dependence:

$$\log D = m + n\rho^{-1} \quad . \tag{7}$$

From her data and Eqs. (1), (4), and (7), one finds

$$A \pm 0.09 = 0.36 - 3.64\,\rho^{-1} \quad . \tag{8}$$

This result is shown in Fig. 22. It is noted that the value for strontium is in good agreement with the other species if $\rho(Sr) = 1.59\ r(Sr^{+2})$.

A report treating diffusion in silicates as it pertains to the fallout problem is being prepared at General Atomic. Included in this report will be a more detailed discussion of the A:B and $A:\rho^{-1}$ correlations and predicted diffusivities for a number of important fission products in at least three silicates.

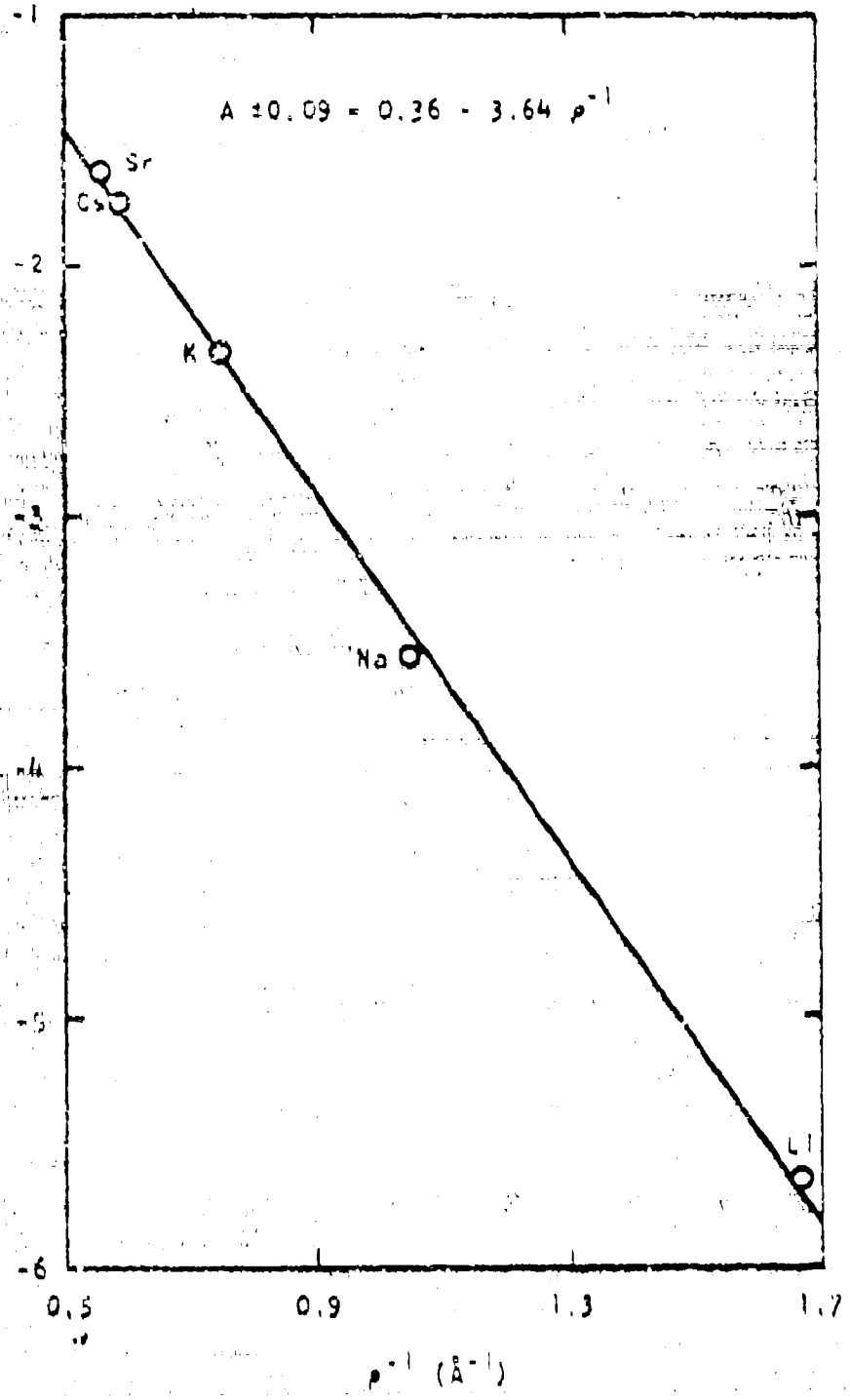

Fig. 22. Correlation between A in log D = A - BT^{-1} with reciprocal effective ionic radius for a low refractory silicate glass. Data taken from Ref. 10

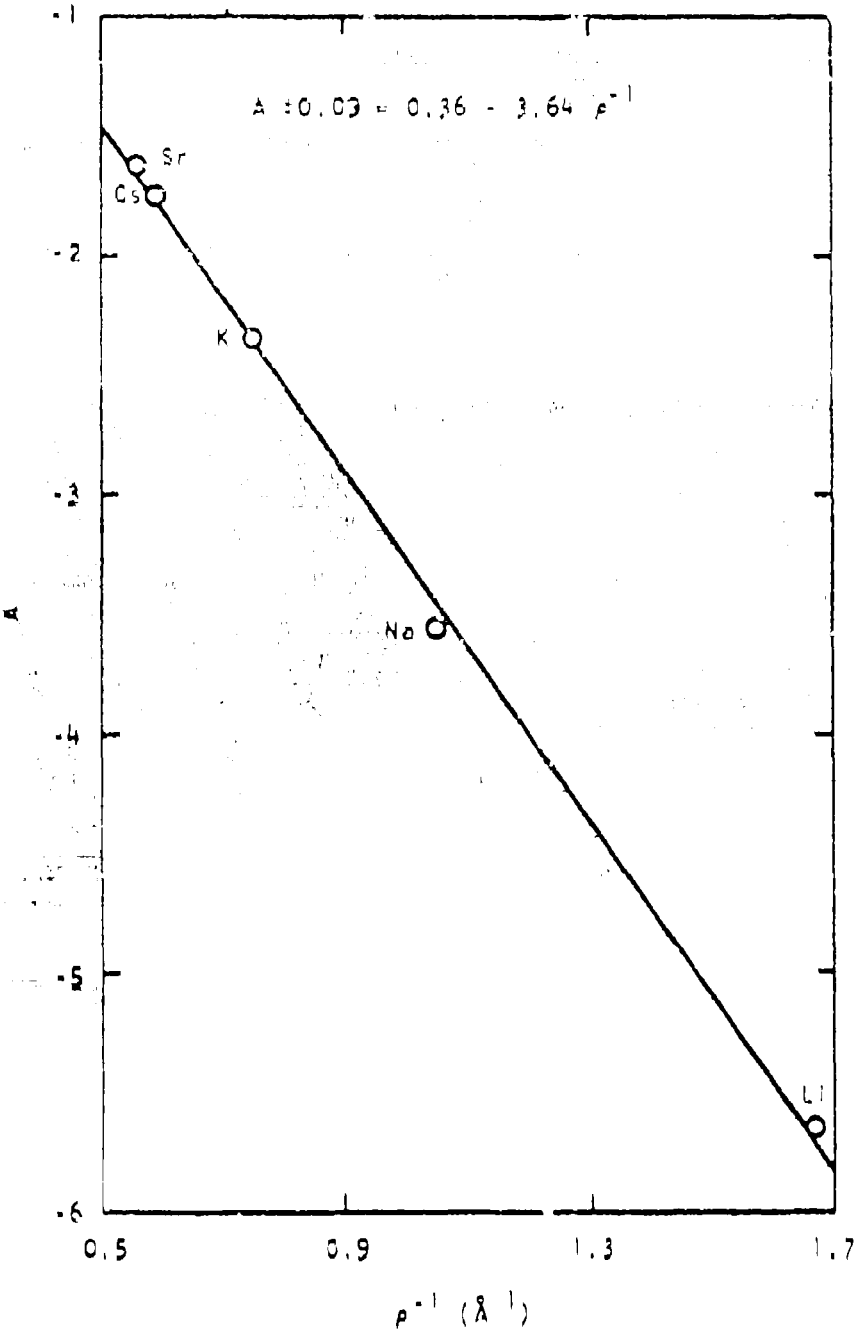

Fig. 22. Correlation between A in $\log D = A - BT^{-1}$ with reciprocal effective ionic radius for a low refractory silicate glass. Data taken from Ref. 10

STUDIES OF THE THERMODYNAMIC PROPERTIES OF GASEOUS SPECIES

INTRODUCTION

Interest in the behavior of cesium and rubidium during fallout formation has led to an investigation of the vaporization of the alkali metal oxides. During the present reporting period, an article entitled "Knudsen Cell Measurements to Determine the Stabilities of Gaseous Cesium and Rubidium" was written.[12] In addition, an article on the gaseous alkali metal oxides is being prepared for submission to the Journal of Chemical Physics.

Silicate studies have been made for the purpose of correlating the gaseous cesium oxide studies with transpiration results presented in the present report.

Mass spectrometric studies of the gaseous cerium oxides have been initiated, and preliminary results are of considerable interest.

GASEOUS ALKALI METAL OXIDES

In 1951 Brewer and Mastick[13] calculated the stabilities of the gaseous M_2O alkali metal oxides. Their results suggest that only Li_2O is stable enough to be easily detected. Indeed, they calculated that the stability of these oxides decreases in the series lithium, sodium, potassium, rubidium, and cesium. Cesium-oxygen bond energy was calculated to be 12 kcal/mole. In studies performed under the present contract, a measured value of 69 kcal/mole was obtained for this energy; that is, gaseous Cs_2O is a reasonably stable molecule. Other $M_2O(g)$ molecules have been experimentally judged to be reasonably stable also, though less

so than Cs_2O or Li_2O. It is believed that the main reason for the high degree of stability lies in the high polarizability of the larger alkali metal ions, as has been suggested by Klemm and Scharf.[14]

The thermodynamics of the gaseous alkali metal oxides is summarized in Table 3, the heats of formation are second law heats and the entropies were derived from relative ionization cross sections and a pressure calibration. The uncertainties in the heats thus must be reflected in the $T\Delta S$ term and an additional uncertainty from the pressure estimates combined with it to give entropy uncertainties. Temperature errors during these studies are believed to be small.

Table 3

THERMODYNAMICS OF FORMATION OF GASEOUS ALKALI METAL OXIDES FROM GASEOUS ELEMENTS

	$-\Delta H_T$ (kcal/mole)	$-\Delta S_T$ (e.u.)	T (^oK)
Li_2O	104.8±1.4	28.7	1500
Na_2O	59.3±2.2	35.9	1100
K_2O	58.2±3.7	36.8	1050
Rb_2O	51.4±3	30.5	1100
Cs_2O	77.1±6.3	34.7	1500
Cs_2O_2	98.6±6.5	53.6	900
CsLiO	(90)		

The Li_2O studies can be compared with those of White, et al.,[15] in which a very similar second law heat was measured but the entropy term was taken not according to cross sections but to Li_2O transport in vaporization experiments. The latter approach apparently is the reason for the differences between the results obtained in the present experiment and the results of White, et al.

The data of Table 3 point out the stability of the alkali metal oxides and suggest a considerably different behavior for cesium and rubidium in fallout formation than had been suggested in the case of low oxide stability.

A more complete description of the findings described above can be found in Refs 12 and 16.

CESIUM SILICATE STUDIES

The results of cesium and rubidium transpiration studies have suggested that an oxidized metal species is important, and the results of mass spectrometric studies have pointed out the importance of the oxide species of these metals. An attempt was made to correlate these studies by observing through mass spectrometry the molecules effusing from an iridium Knudsen cell in which cesium oxide was dissolved in a calcium aluminum silicate sample. Gaseous species recognized in this study were Cs, Cs_2O, Cs_2SiO_3, Cs_2MoO_4, and $CsIrO_n$ (where n = 3 and possibly less). The Cs_2MoO_4 was from a molybdenum cell contaminant. Expecting the Cs to be the dominant cesium gaseous species during fallout formation seems unrealistic, since it has been determined that the cesium-oxygen bond energy is 69 kcal/mole. This is sufficient reason to believe that cesium in an oxidizing atmosphere at temperatures of interest to fallout formation (1000° to 2000°K) will tend to be bound to oxygen in some way.

On the basis of the mass spectrometric work performed, it appears that a molecule similar to the cesium silicate gaseous molecule may be important to fallout formation. Cesium hydroxide should also be considered as a gaseous species possibly important in fallout formation.

CERIUM OXIDE STUDIES

White, et al.,[17] reported the presence of $CeO_2(g)$ in a study of the vaporization of $CeO_2(s)$. The presence of this species has been confirmed

in this Laboratory. In fact, when an iridium Knudsen cell initially containing $CeO_2(s)$ was used, $CeO_2(g)$ was the only species observed to be effusing from the cell. Over $Ce_2O_3(s)$ the species CeO(g) has been observed, and over Ce_2O_{3+x} both CeO(g) and $CeO_2(g)$ have been observed. Measurement of the stability of $CeO_2(g)$ by proper chemical manipulation is planned.

A CONDENSED STATE, DIFFUSION-LIMITED MODEL OF FISSION PRODUCT ABSORPTION IN FALLOUT

In the last report,[2] it was stated that it seemed possible to construct a mathematical model employing diffusivity as rate limiting in the absorption of fission products during fallout formation. A report has since been prepared which describes such a calculational program.[6] The basic calculations involve a time-temperature stepping system with mass balances made at each step, in which the surfaces of all particles are assumed to achieve equilibrium with the gas phase but the penetration of fission products into (or out of) the fallout particle is considered to be diffusion-controlled. This is done for a field of various-sized silicate fallout particles which are assumed to be nonvolatile, internally nonconvecting, and nonagglomerating. Fission products are decayed after each time-temperature step, and up to six isotopes in a decay chain can be handled. Cloud temperatures are taken to be homogeneous in the expanding cloud volume, as also are particle distribution and gaseous fission products. Cloud volumes and temperatures are provided to the system as step functions of time as determined by the yield of the device. Fission product yields, cloud soil content, initial temperature, final temperature, and temperature intervals are also input information.

Some of the results of sample calculations obtained using this program are also considered in this report. In these calculations examples of a refractory and a volatile chain, 95 and 137, respectively, were selected for study. The results should demonstrate the difference in behavior for extreme cases with varying conditions and thus provide limits of behavior. In these sample calculations, fireball volumes were scaled according to

Miller's description;[18] the standard amount of soil brought into the cloud was also scaled according to a description by Miller,[18] the standard particle distribution was developed from one used by Miller;* Henry's law constants were taken from Norman;[5] experimental and estimated diffusion coefficients were employed as measured or estimated in studies reported here and in a previous report;[2] initial fission product yields were taken according to Crocker;[19] half lives were taken from Crocker, Scheidt, and Conners,[20] and total fissions were scaled as a function of weapon fission yield according to Miller.[18]

Several program variables were investigated in order to demonstrate the degree of dependence of the calculational system on these variables. For instance, the variation of results with the size of the temperature increment must be vanishingly small for the selected temperature increment as smaller increments are considered. Also, the variation of results with choice of initial and final calculational temperatures should be defined. Finally, the fact that the particle size distribution employed is idealized—that is, some selected radii represent all of the mass of the particles—was considered. These points were investigated and seem to be satisfactorily understood as is demonstrated in this report.

This investigation demonstrated the effects of condensed state diffusion in a fallout calculational model embodying this phenomenon. It is interesting to compare results using this system with the Miller model,[18] where diffusion is deemed infinitely fast above 1673°K and negligibly slow below this temperature. For the case of the highly absorbed nuclide chain, the only noticeable difference is that the calculations for the larger particles in the diffusion-controlled model suggest that equilibrium conditions may not be attained by these particles during fallout formation. Equilibrium conditions are assumed by Miller. In the case of a volatile chain, the diffusion model predicts an absorption behavior which varies with particle

*Miller, C. F., private communication, November 1965.

size. Miller's model assumes no absorption difference with particle size. In the diffusion model, cooling rate will slightly affect absorption, while in Miller's model it will affect absorption only to the extent that this quantity interacts with fission product decay. Radial concentration gradients are predicted and demonstrated in the calculational report within a fallout particle with the diffusion model, while with Miller's model there are no concentration gradients within a particle, only at the surface of the particle. It seems reasonable to state that the diffusion model provides a more revealing and perhaps a more accurate calculational tool for considering fallout. It is, however, a limited model, and the assumptions underlying the development of the model should not be ignored.

ELECTRON MICROPROBE STUDIES

During the present reporting period, electron microprobe studies on sectioned collected fallout were continued. Previously, inhomogeneities, examples of accretion events, and lead coats for particles from shot Johnie Boy had been demonstrated.[2] As a result of those studies, it was proposed that an Eniwetok detonation that was seeded with various minerals be investigated specifically to determine the distribution of these minerals. The results of this investigation are described below.

On the ground under a relatively small tower shot, large quantities of the minerals $KAlSi_3O_8$, $BaSO_4$, SiO_2, TiO_2, and $ZrSiO_4$ were spread. These minerals were incorporated into the nuclear cloud and became distributed in the fallout from this cloud. A bottle of coral sand and fallout was obtained from C. E. Adams of USNRDL for the purpose of studying the seeding elements in the fallout.

Fallout particles in the coral sand could be recognized using autoradiographic techniques. By using these techniques and developing some familiarity with the appearance of fallout particles, most of the radioactivity in the sand could be selectively removed with a relatively small number of particles. A total of 75% of the Co^{60}, 55% of the radioisotopes (Eu^{155}, etc.) causing the 0.080 MeV radiation, and 17% of the Cs^{137} was removed in this fashion. The Cs^{137} appeared to be rather generally distributed in the coral sand as if it were mainly deposited on the sand itself. This might have occurred when Xe^{137} decayed to Cs^{137} and deposited on the sand or possibly on some tarry material which later became associated with the sand. (A tarry, HCl incoluble material was found to contain considerable Cs^{137}.)

Three types of fallout particles were recognized:

1. Black spheroidal particles, often ceramic coated.
2. Ceramic spheroidal particles varying in color. Several particles were often found fused together.
3. Irregular ceramic particles where coral sand had apparently been exposed to a heat (and fission product) flux but not to the extent that the particles totally melted.

The irregular particles were more numerous than the ceramic spheroids and the ceramic spheroids were much more numerous than the black spheres; in a given sample, they were found in the ratio 160:130:30, respectively. Of the radioactivity in the described sample, the black spheroids contained 25%, 40%, and 4%, the ceramic spheroids 32%, 17%, and 5% and the ceramic irregular particles 18%, 9%, and 7%, respectively, of the isotope Co^{60}, the isotopes giving the 0.080 MeV γ, and the isotope Cs^{137}.

Microprobe studies supported the belief that the irregular particles were partially fused coral sand. The surface layers of these particles generally contained tower iron in the form of iron droplets and/or a diffuse surface layer of this element. The seeding elements, potassium, aluminum, barium, sulphur, silicon, titanium, and zirconium, were discovered in these particles only in very small amounts near the surface. A photomicrograph of an irregular particle highly loaded with iron is shown in Fig. 23a. Figure 23b is an electron backscatter microprobe picture and Fig. 23c is an Fe K_α microprobe picture of the same particle. The microprobe pictures are taken by scanning an exciting, highly focused electron beam over the surface of the particle and photographing the face of an oscilloscope, where the particle response to the exciting electron beam is presented as a function of position on the face of the particle. In Fig. 23b, the intensity of the backscattered electron signal can be observed. This signal is a sensitive measure of the molecular weight and topography of the species being bombarded. In Fig. 23c, the intensity of the K_α X-ray

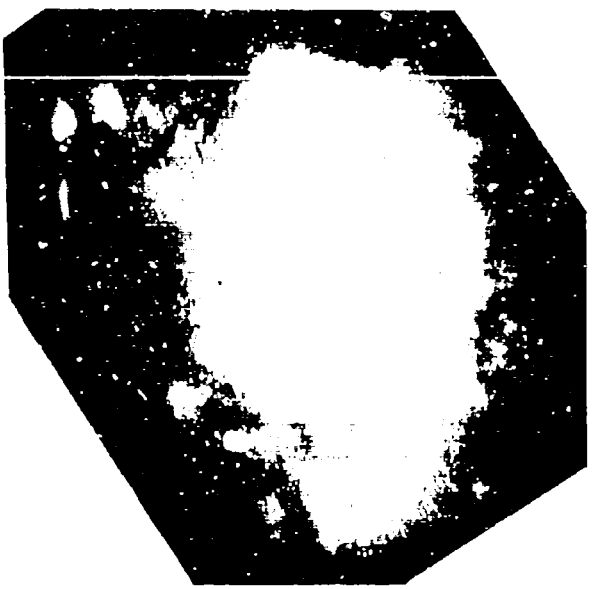

(a)

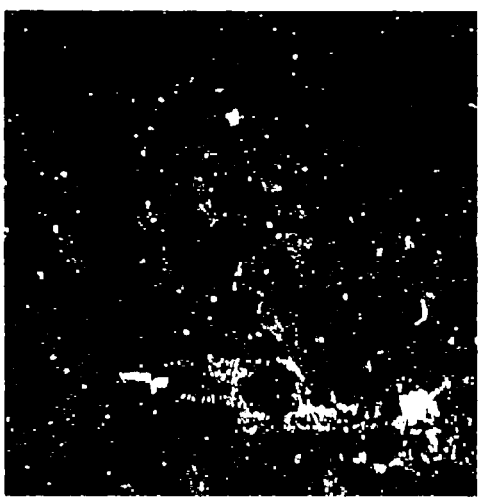

(b)

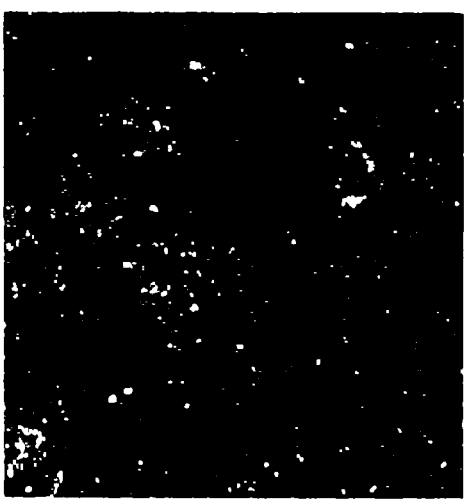

(c)

Fig. 23. Photographs of a sectioned irregular particle: (a) photomicrograph; (b) electron back scatter picture, field ~250 μ × 250 μ (all microprobe pictures are this field unless otherwise stated); (c) Fe K_α picture

radiation from iron present in the sample is presented on the scope as a function of electron beam position.

The results shown in Fig. 23 provide a good description of the particle. The microphotograph indicates a brilliantly white particle core surrounded by a darker band of material which is in turn surrounded by the mounting resin. The particle core has been found to be a material with a high calcium content ($CaCO_3$, CaO, or $Ca(OH)_2$). The electron backscatter picture is presented mainly to demonstrate the boundaries of the particle. The Fe K_α picture was taken with the sample oriented identically as in Fig. 23b, so that superposition of these two pictures provides proper positional information. Note that the high iron areas near the surface seem to be coated. Also, the presence of some iron-rich spheroids in the iron layer is apparent. This particle thus would seem to represent an incompletely melted grain of coral sand, bombarded first with tower debris and then coral sand debris. A more typical irregular particle would not exhibit as much iron or as heavy a final calcium coat.

Another iron boundary is demonstrated in the Fe K_α picture of another particle with a high iron content shown in Fig. 24. This picture clearly demonstrates the frequently encountered directional nature of the iron coating.

The ceramic spheroids possessed very many more particle structure features than the irregular particles, but these particles also did not contain sufficient quantities of seeding elements to warrant extensive study. The particles shown in Figs. 25 through 28 are interesting examples of this type of particle.

The bright area in Fig. 25a appears to be similar to the central regions of the particle in Fig. 23a and corresponds to a high calcium phase. Two darker spherical-appearing portions at either end of the particle and other irregular features can be distinguished in Fig. 25a. The portions of the particle with high electron backscattering are shown in Fig. 25b; the iron distribution in the particle is shown in Fig. 25c. The two large,

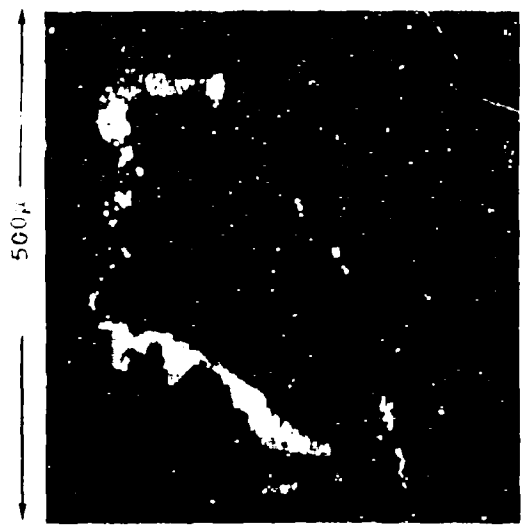

Fig. 24. Fe K_α picture of a sectioned irregular particle

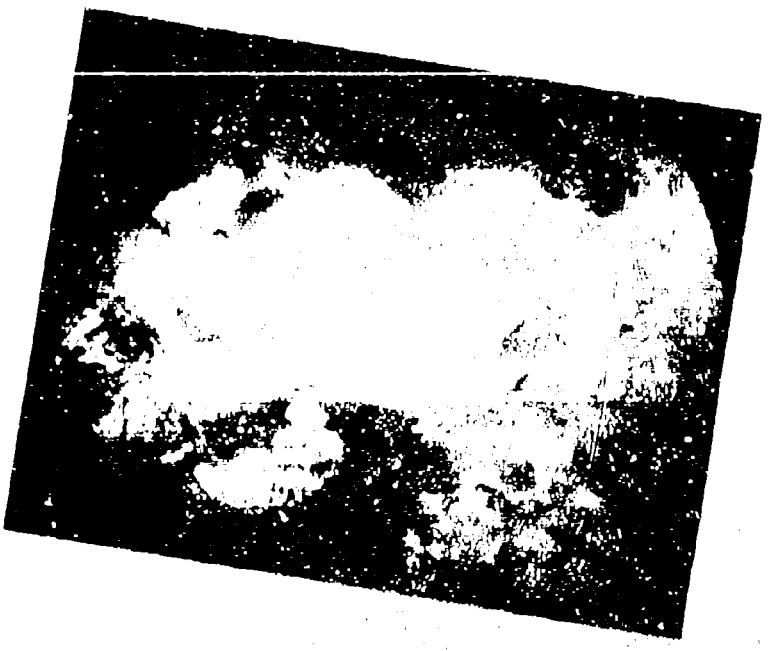

(a)

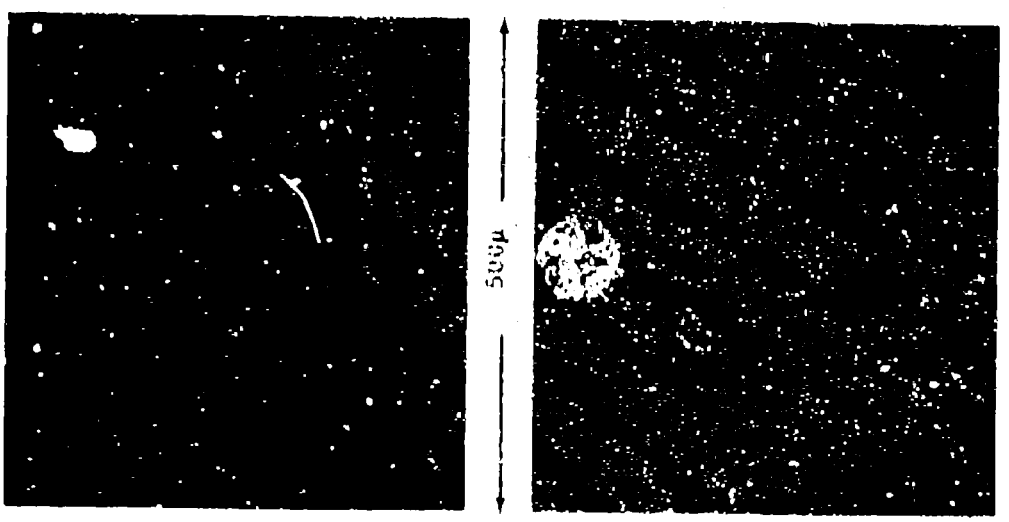

(b) (c)

Fig. 25. Photographs of a sectioned "spheroidal ceramic" particle. (a) microphotograph; (b) electron backscatter picture; (c) Fe K_α picture

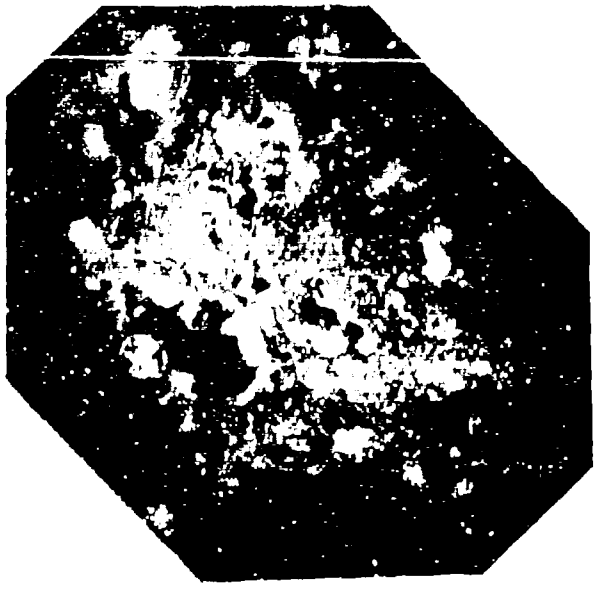

(a)

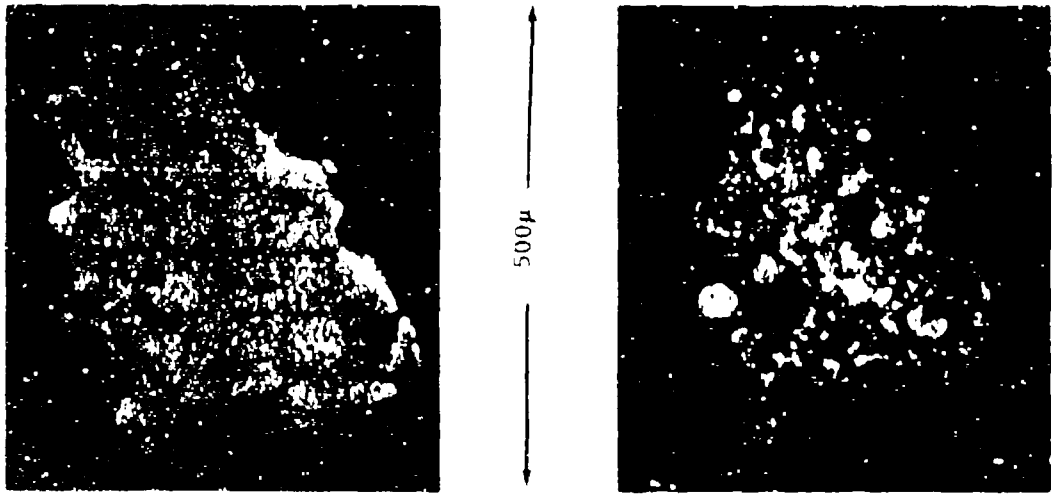

(b) (c)

Fig. 26--Photographs of a sectioned "spheroidal ceramic" particle: (a) microphotograph; (b) Ca K_α picture; (c) Fe K_α picture

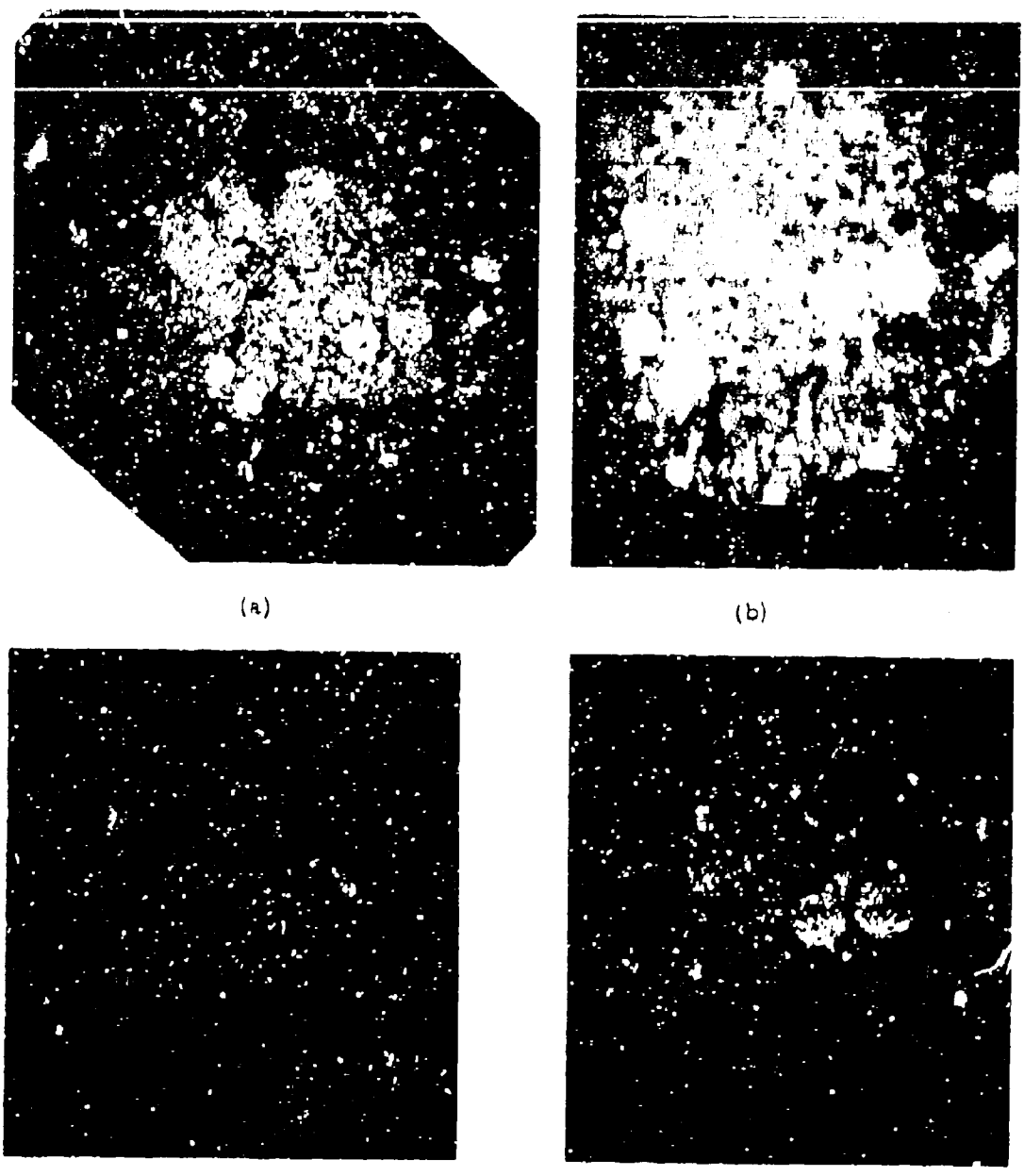

Fig. 27. Photographs of a sectioned "spheroidal ceramic" particle: (a) microphotograph; (b) electron back scatter picture; (c) Ca K_α picture; (d) Fe K_α picture

Fig. 28. Electron back scatter picture of a sectioned "spheroidal ceramic" particle

iron-rich spheres seen in the microphotograph are also demonstrated in Fig. 25c. This Fe K_α picture definitely indicates the importance of agglomeration processes occurring in fallout formation.

Figure 26 also demonstrates the agglomerative phenomenon in fallout. Note that in these pictures the boundaries of the particle extend beyond the high iron areas. Also, spherical iron inclusions can be seen in the particle (as can some iron inclusions that are not spherical).

Figure 27 shows another particle which has experienced a high degree of agglomeration. The Fe K_α and Ca K_α pictures are very representative of agglomeration of high Ca-Fe spheres in a calcium-rich matrix. Again, the seeding elements could at best barely be detected.

Figure 28 is an electron backscatter picture of an interesting particle where two large, calcium-iron-rich spheroidal particles agglomerated and then were coated by a high calcium phase.

A study of this type of ceramic particle emphasizes the importance of agglomeration. These particles generally seem to be agglomerated from smaller particles and often are coated with a high calcium phase. While the particles appear to have been molten, it seems obvious that some solidification occurred before agglomeration. Particle solidification behavior according to the phase diagram would be unlikely to result in the spheroidal $2(CaO) \cdot Fe_2O_3$ inclusions observed. The lowest melting phase in the particles would appear to be the iron-calcium-containing phase of which the spheroidal inclusions seem to be made. This might suggest that the presumably more refractory particle coating was acquired after solidification and particle agglomeration occurred. Certainly, much information about fallout formation phenomena can and needs to be derived from ceramic particle studies such as those described here.

Study of the black spheroidal particles provides more insight into the fate of the seeding elements. Over 40 black spherical particles have been subjected to microprobe investigation. This group of particles can be classified as two magnetite particles (Fe_3O_4) which are very low in

calcium and seeding elements; a few particles exhibiting very unusual features, such as a major accretion event; nine well formed, dense particles showing strong evidence of dendritic precipitation of a calcium (oxide) rich phase; five more particles with many of the properties of the nine particles just described, but generally not as well formed; and the remaining particles, which appear to be to a greater or lesser degree porous precursors of the well formed, dense, dendritic type particles. Seeding elements have been found in many of these particles, and the well formed, dense particles characterized by their dendrites are relatively rich in these elements.

Further consideration of the dendritic-type particles yields very interesting information. The refractory seeding elements are found nearly uniformly distributed in the prominent $2(CaO) \cdot Fe_2O_3$ phase of these particles, and the accompanying dendritic, high calcium (CaO) phase is found to be nearly devoid of seeding elements, as would be expected if it is a precipitated phase. Also, no two particles appear to have the same concentrations of seeding elements. The seeding elements sulphur and potassium behave somewhat differently from the refractory elements and generally seem to be found in segregated areas, often near the surface of a particle. Occasionally, one can distinguish seeding minerals themselves For instance, barium was found to be more concentrated in an area near the surface of a dendritic-type particle, where the sulphur content was also high. Spots of silicon were also encountered. The concentrations at which the seeding elements are present in the $2(CaO) \cdot Fe_2O_3$ phase of these particles generally range up to a few percent for a particular element. Some of these particles contain several of these elements in relatively high concentrations.

In Figs. 29, 30, and 31 the progression from porous, cracked particles to dense, dendritic-type particles is shown. The particle shown in Fig. 29 appears to be severely cracked and has a large tear hole in the center. The cracks are apparent even in the Ca K_α picture, where cracks

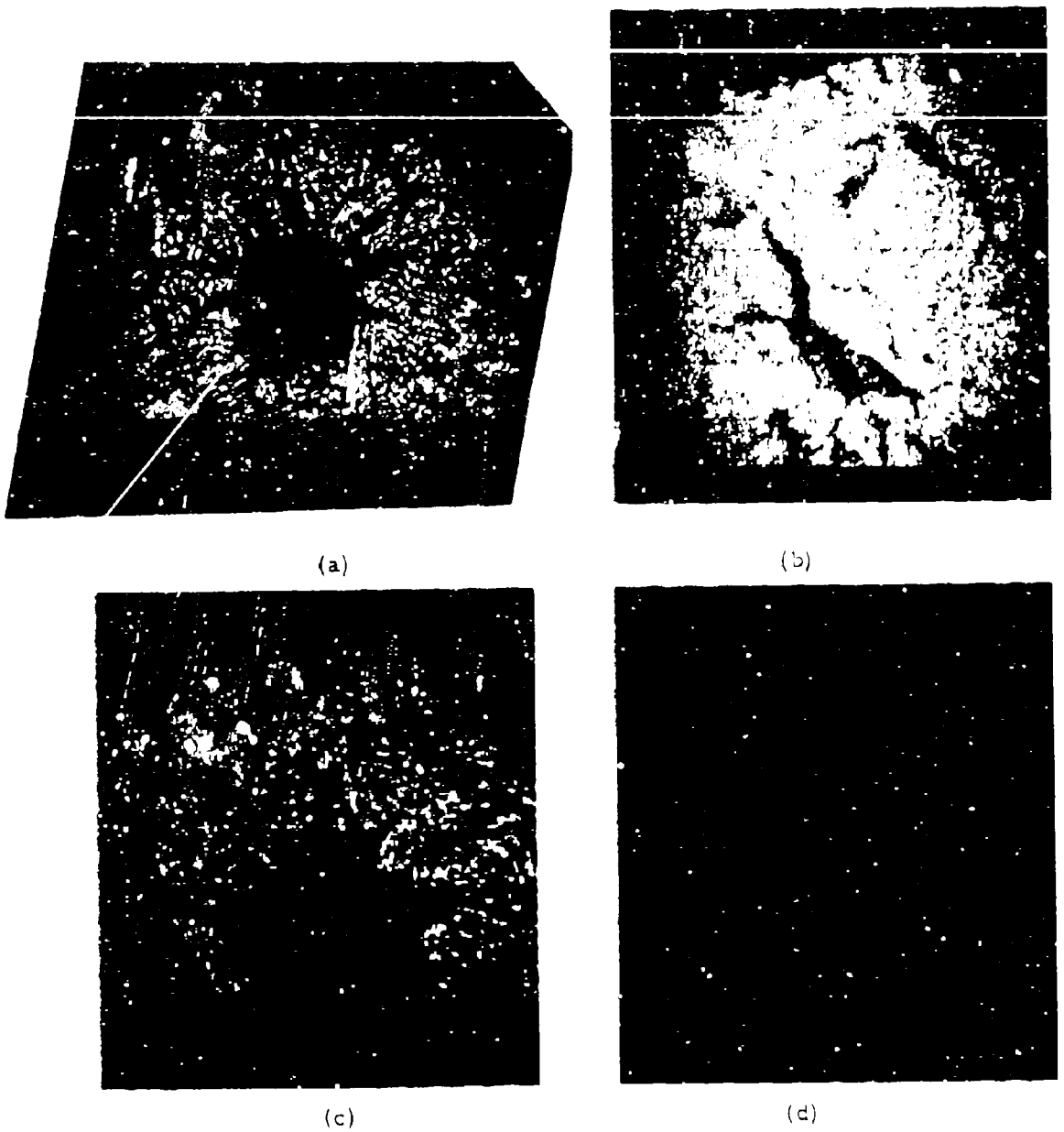

Fig. 29. Photographs of a sectioned black spheroidal particle: (a) microphotograph; (b) Ca K_α picture; (c) Fe K_α picture (d) Si K_α picture

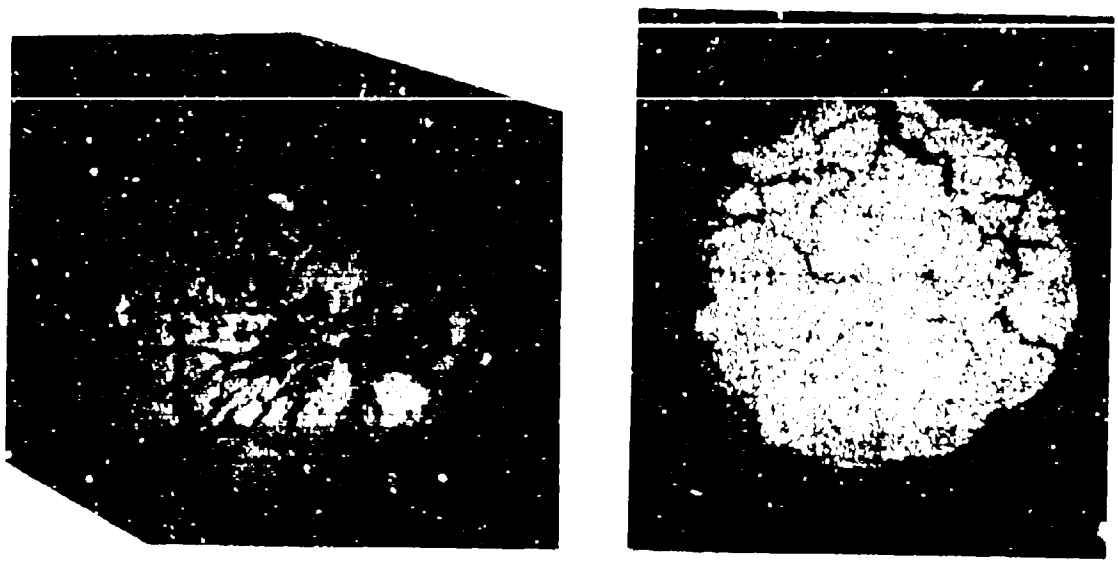

(a) (b)

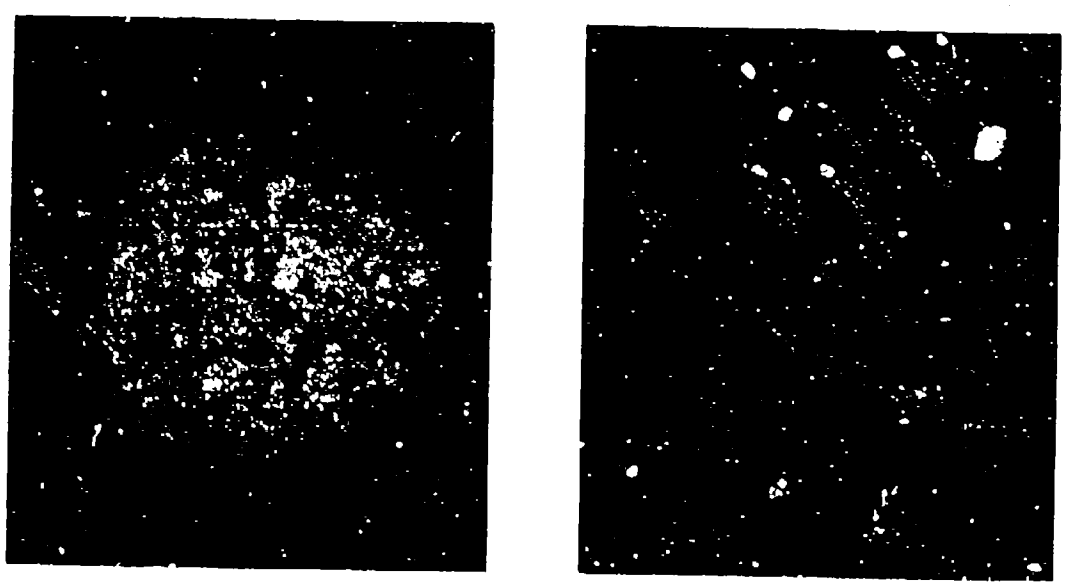

(c) (d)

Fig. 30. Photographs of a sectioned black spheroidal particle: (a) microphotograph; (b) Ca K_α picture; (c) Fe K_α picture; (d) Si K_α picture

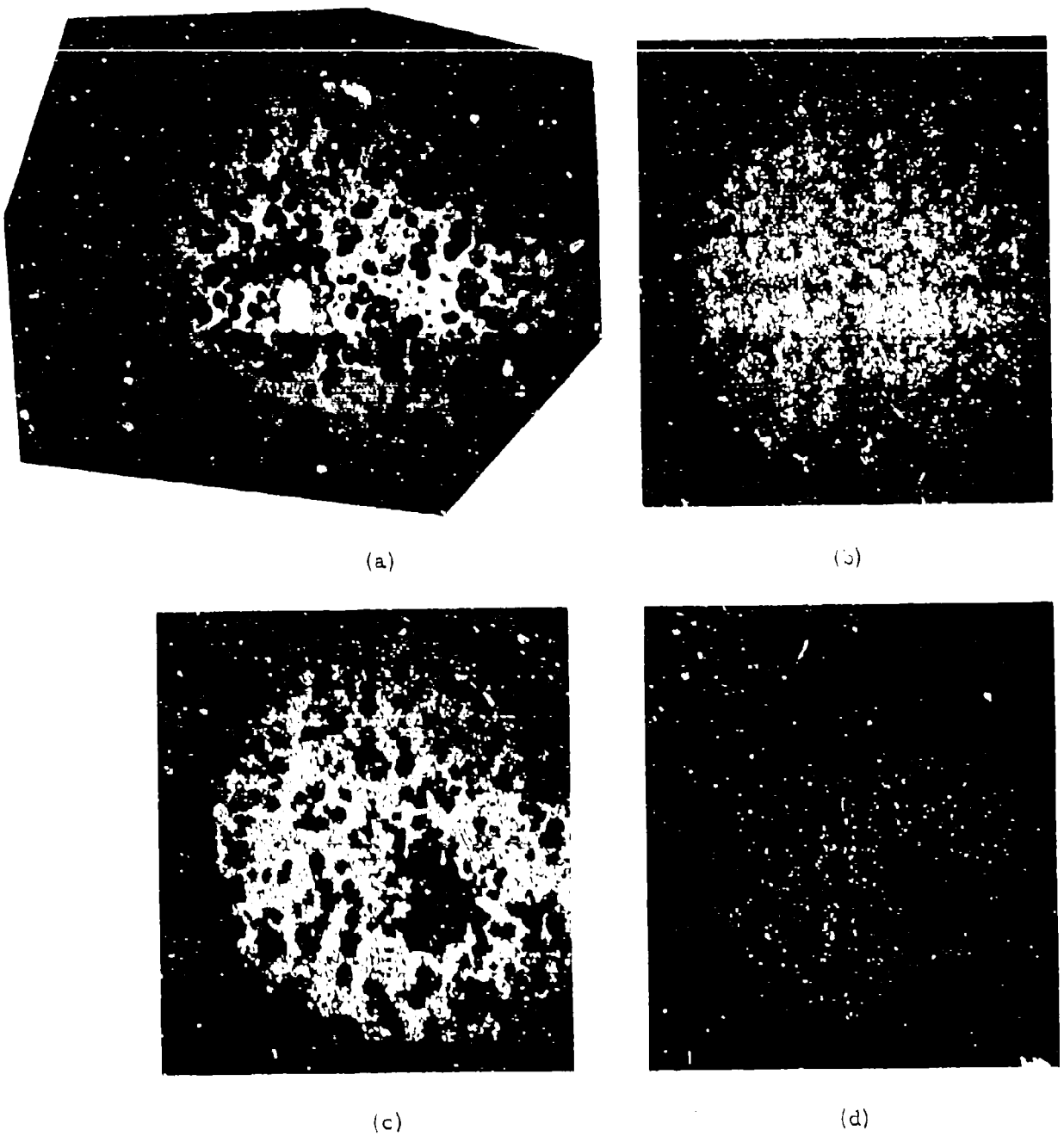

Fig. 31. Photographs of a sectioned dendritic black spheroidal particle: (a) microphotograph; (b) Ca K_α picture; (c) Fe K_α picture; (d) S: K_α picture

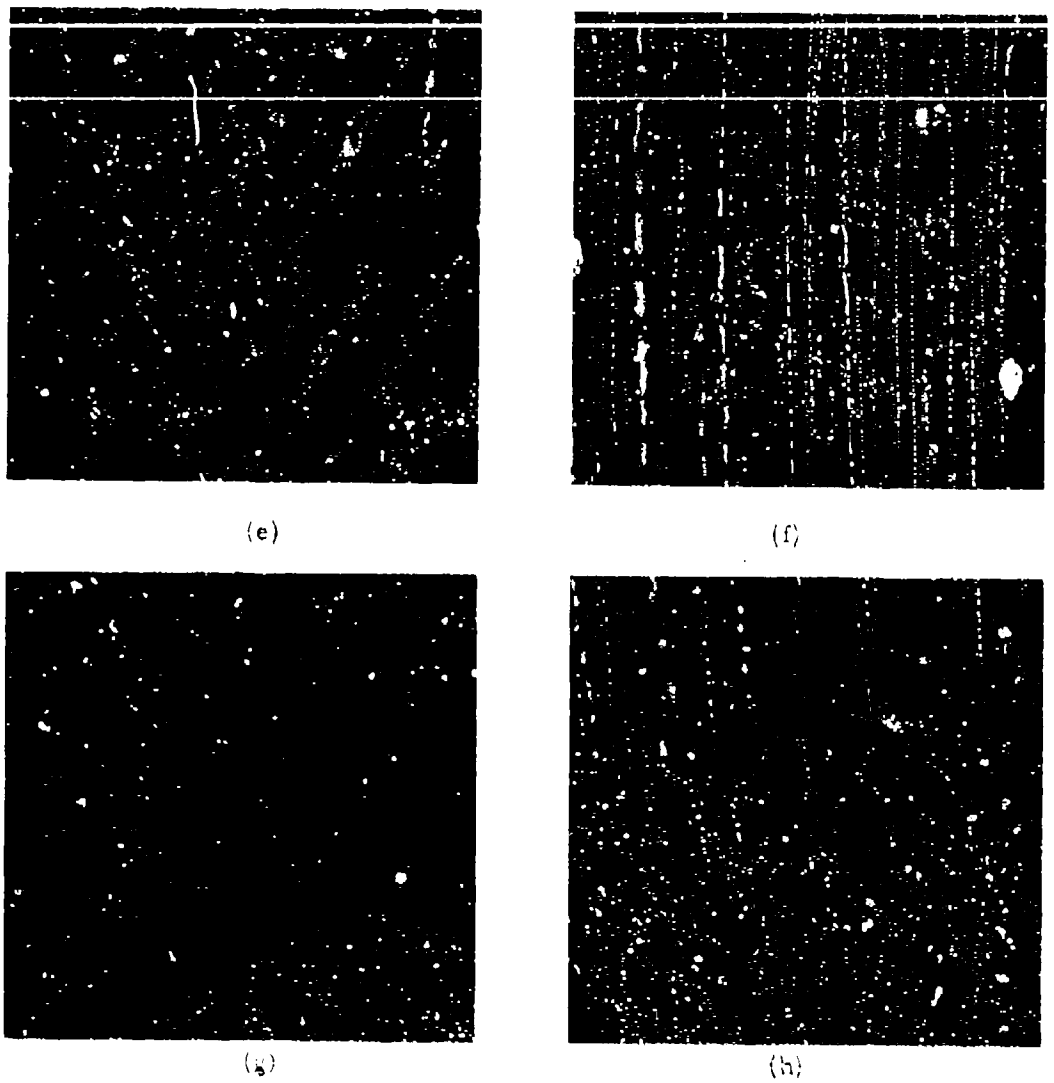

Fig. 31. Photographs of a sectioned dendritic black spheroidal particle: (e) Zr L_{α} picture; (f) Ti K_{α} picture, (g) Ba L_{α} picture; (h) S K_{α} picture

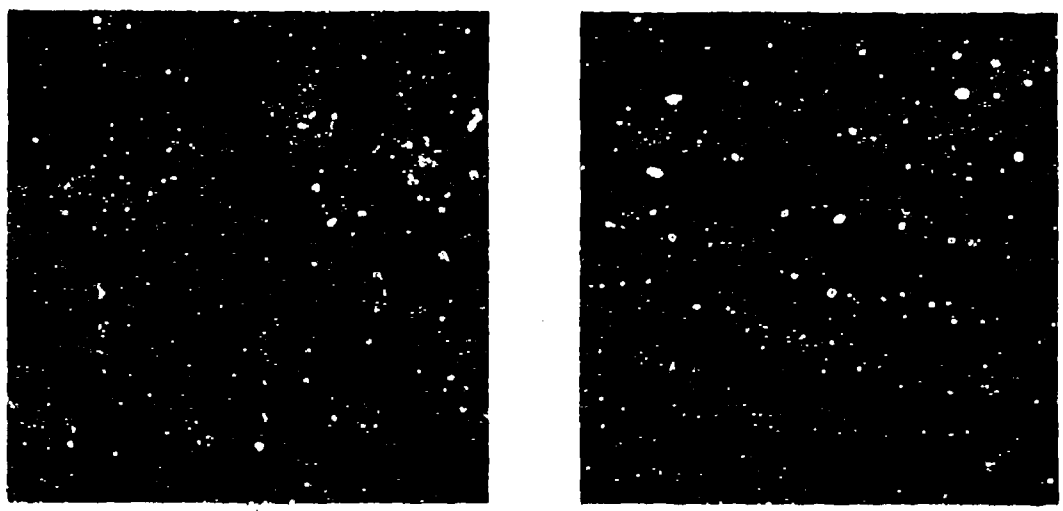

(i) (j)

Fig. 31. Photographs of a sectioned dendritic black spheroidal particle: (i) Cl K_α picture; (j) K K_α picture

must be fairly deep before they can be observed. Note that the tear hole detail does not appear clearly in the Ca K_α picture but does in the Fe K_α picture. In the Si K_α picture of this particle, a few small high-silicon specks appear on the sectioned face. Figure 30 shows a particle with few dendrites, some cracking, and silicon spots. The silicon, however, does show some tendency toward homogeneity. The particle shown in Fig. 31a exhibits a well formed dendritic structure. Most of the seeding elements have been easily detected in this particle. Figures 31b through 31j show elemental distributions. The Ca K_α picture and the Fe K_α picture indicate that the dendrites are a calcium-rich, nearly iron-free phase (CaO), while the matrix is apparently a $2(CaO) \cdot Fe_2O_3$ phase. The dendrites suggest that the particle, whose total composition is rich on the CaO side of $2(CaO) \cdot Fe_2O_3$, was at one time molten. On cooling, the CaO dendrites probably precipitated until reaching the temperature at which the eutectic matrix solidified. The eutectic matrix is indeed close to $2(CaO) \cdot Fe_2O_3$ in composition.[21] The refractory seeding elements silicon, zirconium, titanium, barium, and aluminum (not shown) have been found in the $2(CaO) \cdot Fe_2O_3$ phase and, within the sensitivity of the probe, are not found in the CaO phase. This does not seem to conflict with the proposed mode of formation. The seeding elements potassium and sulphur (and chlorine) have also been traced in this particle. These elements are associated with a surface feature; the potassium and chlorine also appear together in one spot internally in the particle; and chlorine in particular appears to some extent in spots throughout the particle. These latter two features are in conflict with the statement that the whole particle was molten. However, since the particle structure is so well defined, it is perhaps plausible that the high potassium and chlorine spots are a contamination problem. The surface feature containing the sulphur, potassium, and chlorine has probably been agglomerated and is not inconsistent with the previous melting argument. If the melting argument is accepted for the case of this particle, it is easy to believe that the particle in Fig. 29 did not

experience this phenomenon since it does not exhibit a well formed dendritic structure and the distribution of the silicon is uneven.

Figure 32 shows more detailed pictures of a repolished surface of the particle shown in Fig. 31. Whereas most of the microprobe pictures in this report were taken of a 250-μ square, these pictures were taken of a 50-μ square. The Ca K_α pictures demonstrate the difference in the calcium concentrations found in the matrix and the dendrites. The Fe K_α picture indicates that the dendrites are low in iron. The Si K_α and the Ti K_α pictures suggest a high distribution coefficient for these elements favoring the iron phase. The Zr L_α and Ba L_α pictures might seem to suggest a slightly lower distribution coefficient, as there is measurable response from the low iron areas; however, much of this signal appears to correspond to background. Some correspondence between barium and sulphur ($BaSO_4$) is demonstrated in these pictures at the surface of the particle, where the barium and sulphur signals are high. Note that sulphur, a volatile element, is not detectible except at the surface of the particle.

In Fig. 33 the particle with the most extensive dendrite structure encountered is shown. These apparently hexagonal, Christmas-tree-like dendrites are also a high calcium, low iron phase. While this particle is not highly loaded with seeding elements, it is apparent in the high magnification pictures of some of the dendrites that at least silicon and titanium are associated with the $2(CaO) \cdot Fe_2O_3$ phase. In the lower magnification pictures the agglomerated and small high iron particles in the coating are noteworthy, as is the dendritic structure.

The information on elemental composition derived in the study of the black spheroids is summarized in Table 4.

There would seem to be two processes by which the seeding elements could be transported to an incipient fallout particle during fallout formation: (1) condensation from the gas phase and (2) agglomeration of particulate matter by a fallout particle. Occurrence of either of these processes while the fallout particle matrix was molten and very mobile could lead to nearly

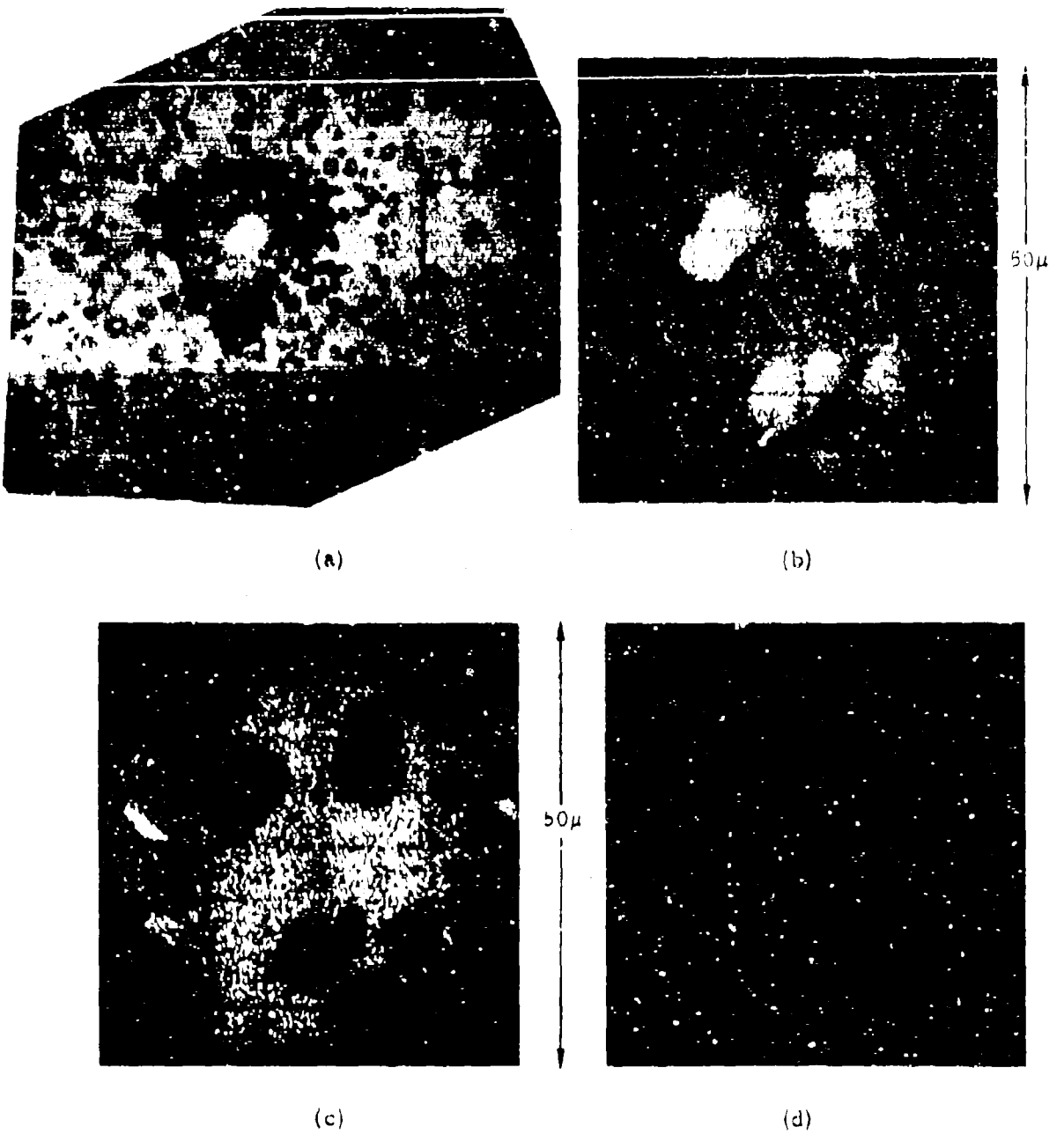

Fig. 32. Photographs of a sectioned dendritic black spheroidal particle: (a) microphotograph; (b) Ca K_α picture; (c) Fe K_α picture; (d) Si K_α picture

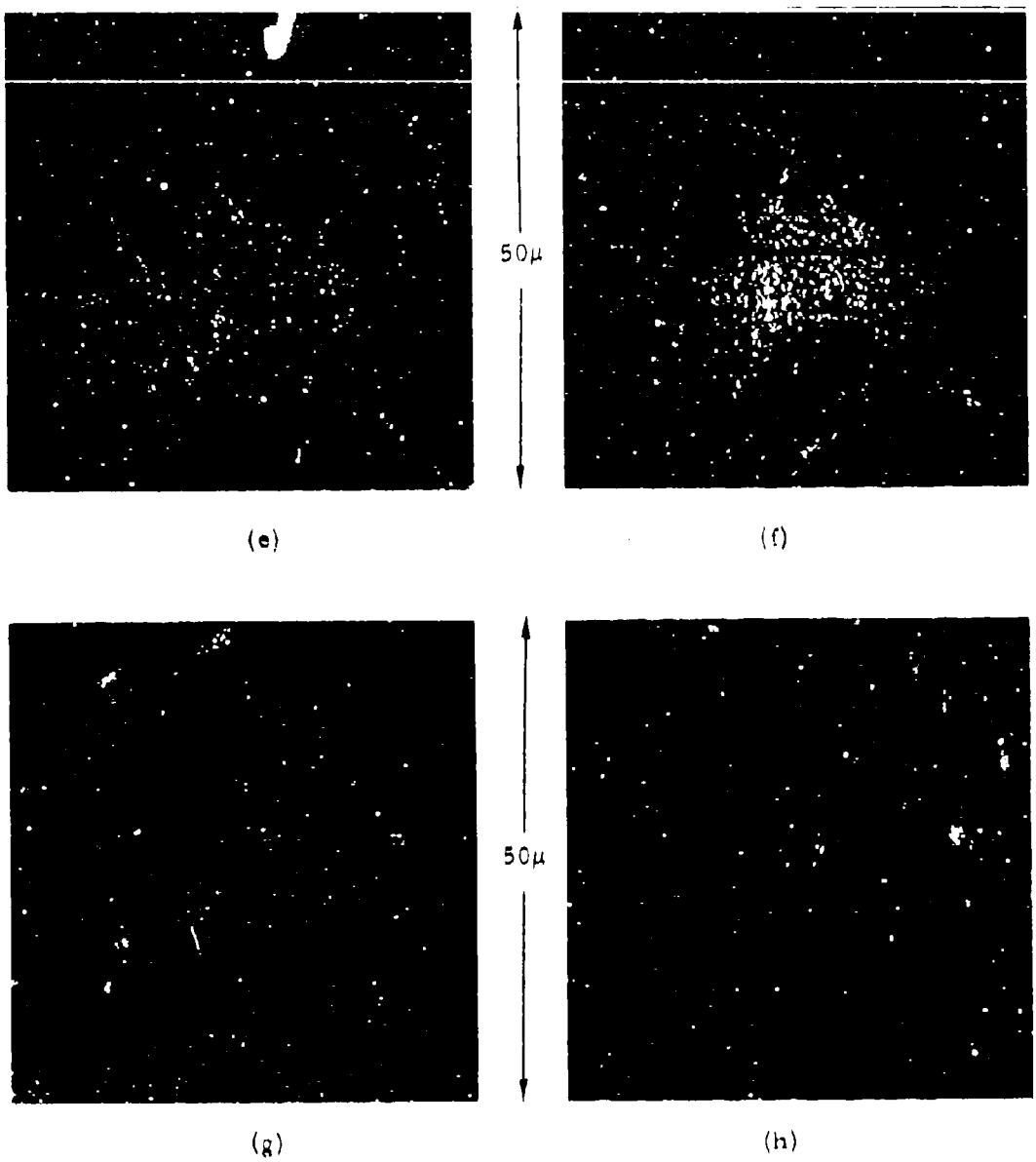

Fig. 32. Photographs of a sectioned dendritic black spheroidal particle. (e) Zr L_α picture; (f) Ti K_α picture; (g) Ba L_α picture; (h) S K_α picture

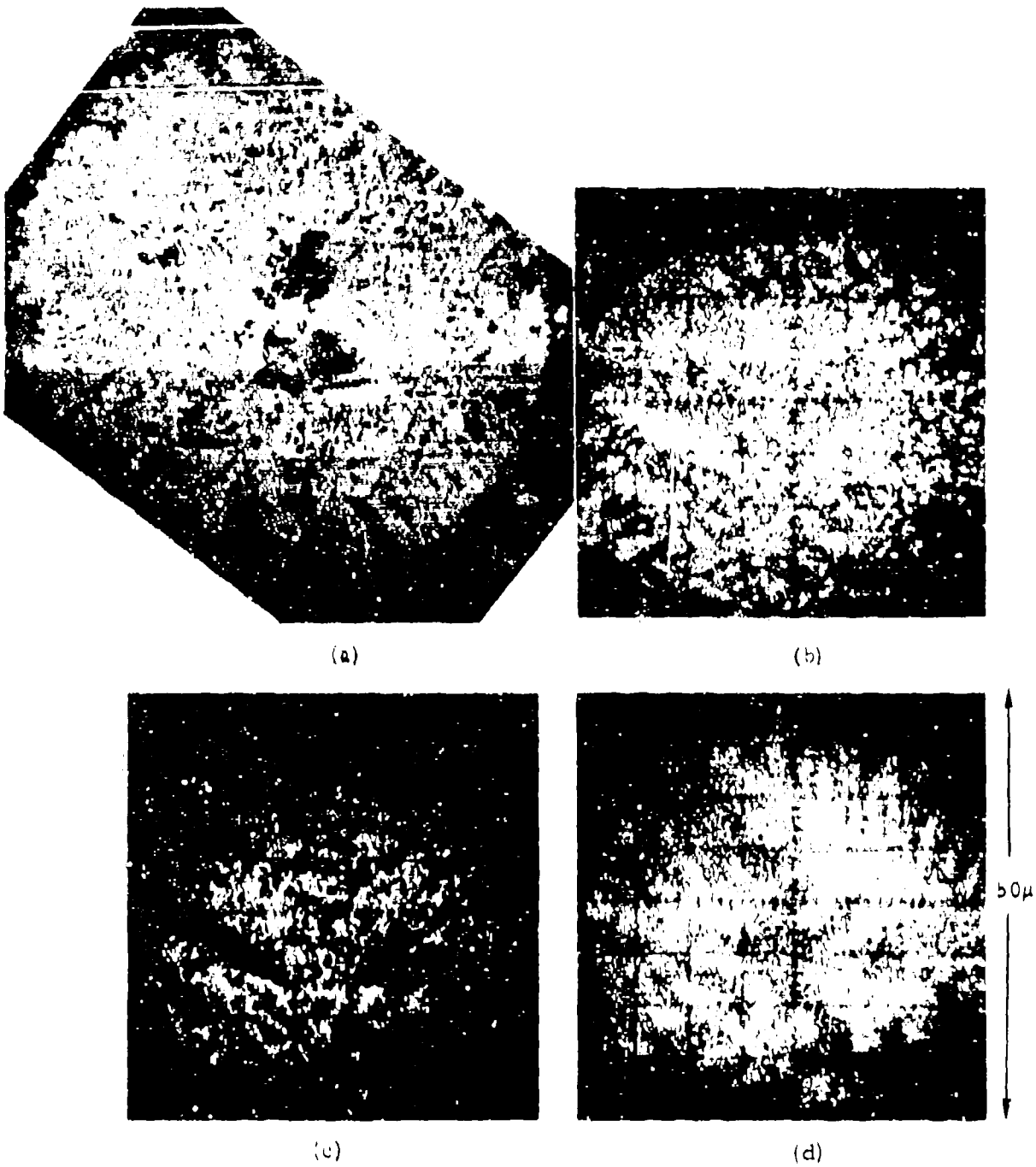

Fig. 33. Photographs of a dendritic black spheroidal particle: (a) microphotograph; (b) Ca K_α picture; (c) Fe K_α picture; (d) Ca K_α picture

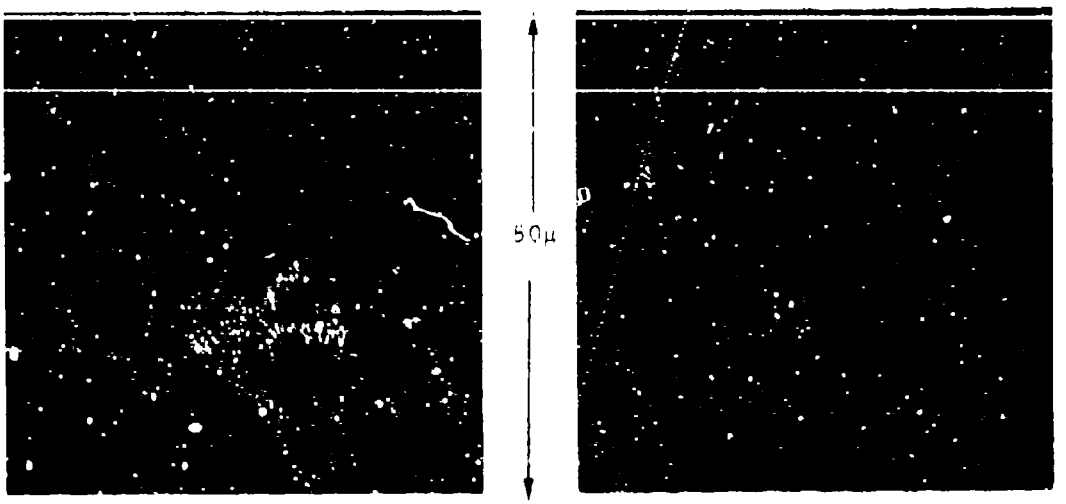

(e) (f)

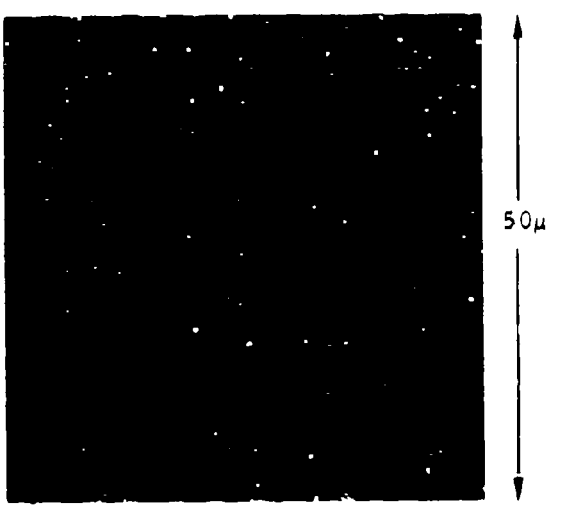

(g)

Fig. 33. Photographs of a dendritic black spheroidal particle: (e) Fe K_α picture; (f) Si K_α picture; (g) Ti K_α picture

Table 4

DESCRIPTION OF BLACK FALLOUT PARTICLES SUBJECTED TO MICROPROBE ANALYSIS

Type	Particle No.	Elements investigated[a, b]									Coating[c]	Remarks
		Si	Ti	Zr	Ba	Al	K	S	Ca	Cl		
Dendritic	A	5	3	2	D	D	D	D	D	C	c	Branching needle dendrites
	B	1	3	B	D	D	D	D	D	BH+G	c	
	C	B	C	D	D	C+G	D	D	D	D	c	(Fig. 33)
	D	1	1	1	D	D	D	BH	D	BH+GH	b	
	E	B+H	B	B	D	D	D	D	D	D	d	Globular needles
	F	2	2	B	C	D	G(Cl)	G	D	GH	b	Globular precipitation
	G	2	B	B	B	B	G(Cl)	G(EC1, Ba)	G	G	g	Globular precipitation (Figs. 31, 32)
	H	B+G	D	D	D	D	D	D	D	D	c	Small globules
	I	A	B	C	C	D	D	D	D	GH	b	Needle-like dendrites
Dendrites abundant	I-0	B+GH	GH	D	GH	C+G(Si)	GH(Cl)	D	G	GH	c	Not as well formed as above particles
	I-1	C	D	D	D	D	D	D	D	D	c	Porous with CaO globules
	I-2	B	B	B	D	D	G(S)	G	G	G	d	
	I-3	3	B	B	C	C	D	G	G	D	d	
	I-4	3	B+GH	B	C	C	D	G	G	D	d	
	0-1	C	D	D	D	D	D	D	D	D	a	Porous with high Ca globules
	0-2	BG	D	D	D	D	D	D	D	D	a	
	0-3	B	D	D	D	D	D	D	D	D	a	Like 0-2 but shows accretion
	0-4	BG	D	D	D	D	D	D	D	D	a	
Odd	0-5	G	D	D	D	D	D	D	G	G	c	Large spherical inclusion
	0-6	D	D	D	D	D	D	D	G	G	d	Conglomerate of small spheres (Fig. 27)
Porous	1	G	D	D	D	D	D	D	D	D	d	Very porous $2(CaO)\cdot Fe_2O_3$
	2	G	D	D	D	D	D	D	D	D	d	
	3	D	D	D	D	D	D	D	D	D	d	Porous $2(CaO)\cdot Fe_2O_3$ matrix
	4	G	D	D	D	D	D	D	D	D	d	

Table 4 (continued)

Type	Particle No.	Elements investigated[a, b]									Coating[c]	Remarks
		Si	Ti	Zr	Ba	Al	K	S	Ca	Cl		
Cracks	5	D	G	D	D	D	D	D	D	D	d	Tear hole, some dendrites
	6	D	D	D	D	D	D	D	D	D	d	Cracked structure
	7	D	D	D	D	G	D	D	G	D	d	Cracks, some dendrites
	8	G	D	D	D	D	D	D	D	D	d	Large tear hole, some dendrites
	9	GH	D	D	D	D	D	D	D	D	c	
	10	G	C	D	D	D	D	D	D	G	d	
	11	D	D	D	D	D	D	D	D	D	d	
	12	BG	G	B	D	D	D	D	D	D	d	
	13	G	D	D	D	D	G(Cl)	D	G	G	a	(Fig. 29)
	14	D	D	D	D	D	D	D	D	D	d	Some dendrites
	15	D	D	D	D	D	D	D	D	D	d	More dendrites, a needle
	16	BG	D	D	D	D	D	D	D	D	d	
	17	G	B	D	D	D	C	D	D	D	c	Tear holes, cracks
	18	BG	C	C	D	D	D	D	D	D	b	Cracks (Fig. 30)
	19	G	D	D	D	D	D	D	D	D	b	
Magnetite	F-1	G	D	D	D	D	D	D	D	D	d	Large hole
	F-2	D	D	D	D	D	D	D	D	D	d	Up to 10% Ca in high Ca areas

[a] A = moderate concentration (1%-5%) in $2(CaO) \cdot Fe_2O_3$ phase
B = low concentration (0.2%-1%)
C = just detectible (<0.2%)
D = not detected
G = a few high spots
H = often near particle surface

[b] Numbers give percents in $2(CaO) \cdot Fe_2O_3$ phase. Elements in parentheses are associated with the element considered.

[c] Coating of particle in the high calcium phase:
a = heavy
b = moderate
c = light
d = not detected

homogeneous distribution of refractory seeding elements in the fallout particles. However, if the gas phase condensation is the important process, the gases in this case were certainly not uniformly mixed, since the particles are generally not similarly loaded. While it is reasonable that the gas phase was not uniform, it seems at least likely that most of the refractory seeding elements have been absorbed into the molten particle mainly by the process of agglomeration. This is strongly indicated by the spots of seeding elements in the particles which apparently have not experienced as drastic a thermal history as have the well formed, dendritic particles.

It is enlightening to reconstruct the histories of the various particles studied. First, the magnetite particles, which should have a melting point of around 1870°K,[21] apparently were not exposed to much hot coral. They must have been formed from the tower and remained in a region essentially devoid of calcium. It is thus likely that these particles were thrown out of the fireball at early times. The well formed dendritic particles encountered considerable amounts of material from the tower and also from the ground. They must have been completely molten (the melting point of $2(CaO) \cdot Fe_2O_3$ is 1450°K[11]) for a relatively long time to uniformly pick up seeding elements. The well formed, large dendrites would seem to indicate relatively slow cooling rates. The observed coatings apparently were laid down after the particles were formed. Other black particles which have small spots of seeding elements rather than dissolved, well distributed large quantities and lack the well formed CaO dendrites, were therefore probably exposed to lesser temperatures for shorter times when the seeding elements were incorporated. The melted, high calcium particles must have encountered a high thermal flux, but the seeding elements were apparently overwhelmed by the amount of coral sand available in the formation of this type of fallout particle. The irregular, high calcium particles were only partially melted, apparently having

been exposed to the mildest temperature histories of any set of recognized fallout particles.

To summarize, it is apparent from the studies discussed above that one should expect to observe particles from a nuclear detonation near a land surface which have widely different compositions reflecting the inhomogeneities of the land surface, inhomogeneities in the cloud, and a considerable degree of agglomeration.

PARTICLE LEACHING STUDIES

SIMULATED FALLOUT STUDIES

Since the diffusion-condensation model will require some leaching phenomena description, it was decided to investigate this problem. A cursory study was initiated using silicate E with radioiodine tracer. The leaching data, which are presented in this section, thus pertain to a special case: a refractory matrix containing homogeneously distributed radioiodine.

A portion of the glass was powdered, passed through a 100-mesh screen, and dried at ~100°C. Weighed samples were placed in double thickness No. 42 Whatman filter papers which were supported in funnels equipped for aliquoting from the tip. Periodically, 5 ml of leachant were added following draining of the previous leachant, and the aliquot was made up to 50 ml and gamma analyzed using reproducible geometry. Leaching was carried out at room temperature without agitation. Because of the low leaching rates, initial leaching times were about 20 min, with the longest experiment lasting 2 days. This interval would seem to be the most important biochemically following ingestion of particles.

The following four leachants were used:

Leachant	pH	Remarks
HCl	?	To represent the human stomach
Tap water	8.3	Colorado River water
Deionized water	7	To represent rain water
NaOH	10	For comparison

Since a surface area measurement has not been obtained for the prepared sample, the results can only be placed on a reciprocal weight basis at this time. By photomicrography, the particles were found to be roughly 100 μ in "diameter."

The leaching data are shown in Fig. 34. It was at first felt that the mechanism of leaching might be diffusion-limited transport of the leachant into the matrix or of radioiodine out through the leachant. If this were the case, since only about 1% of the activity was removed, leaching should be proportional to $t^{1/2}$ (Fick's law). This dependence was not observed. However, the data can be described by the Elovich equation, which has found wide application in chemisorption:[22]

$$\frac{dQ}{dt} = a \exp(-\alpha Q) \ , \tag{9}$$

where Q is the amount of material desorbed (sorbed), t is time, and a and α are constants at fixed temperature. By assuming that Q = 0 when t = 0, the integrated form can be written

$$\alpha Q = \log_e (1 + a\alpha t) \ . \tag{10}$$

The present data can be fitted to Eq. (10) by using the values of a and α given in Table 5.

Table 5

COEFFICIENTS FOR THE ELOVICH EQUATION AT 300°K

Leachant	$a \times 10^{-2}$	$\alpha \times 10^{3}$
pH = 7	3.33	2.33
pH = 10	2.32	1.25
pH 2	8.77	1.08
Tap water	6.62	1.15

The data fitted in this manner are shown in Fig. 35, where it is seen that their agreement with the Elovich equation is good. Leaching data reported by other laboratories[23-25] can also be fitted to this equation. The fact that leaching data can be fitted to the Elovich equation, at least for short times, should be regarded as a phenomenological result

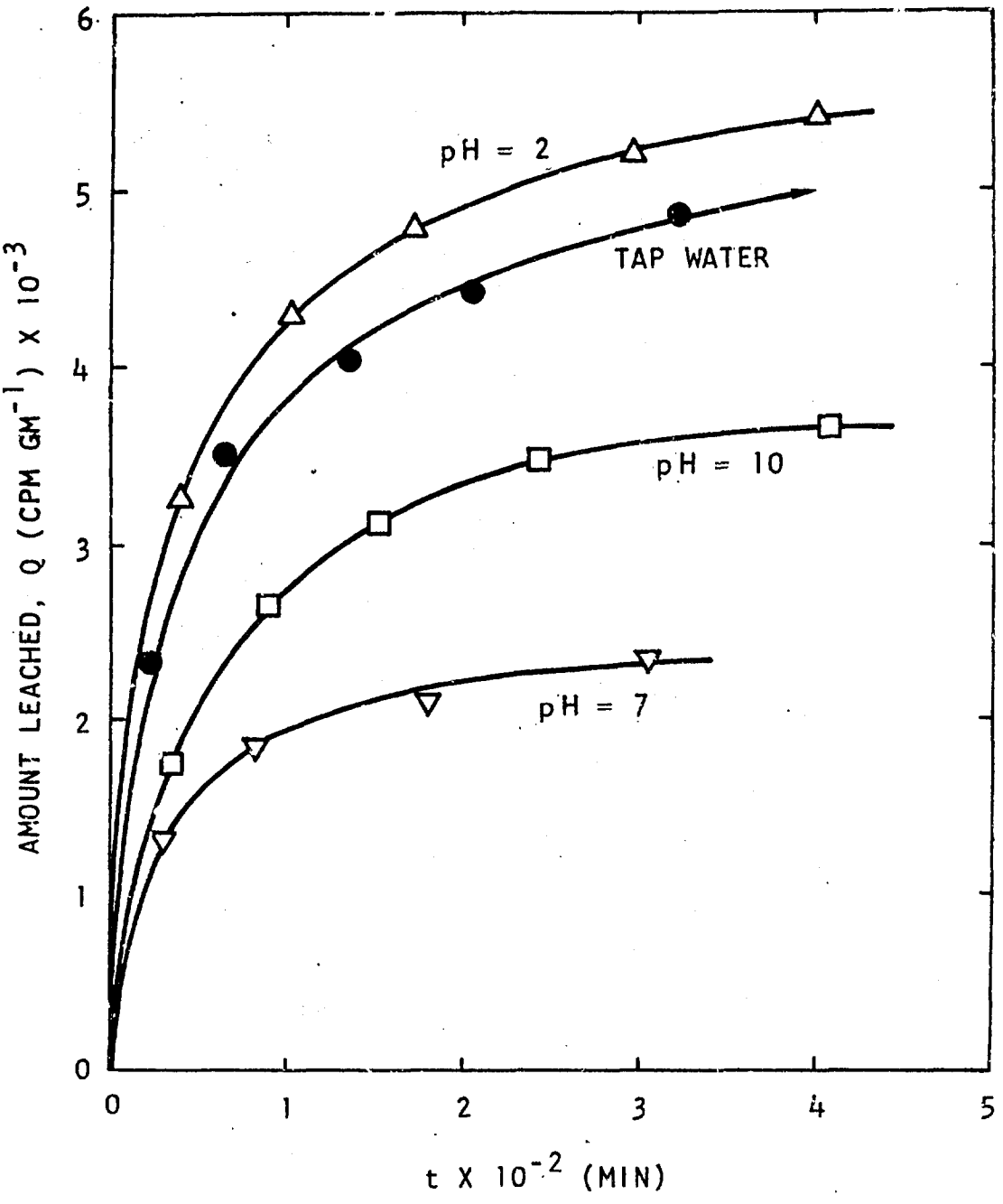

Fig. 34. Leaching of radioiodine from powdered 1450°K eutectic $CaO\text{-}Al_2O_3\text{-}SiO_2$ doped with I^{131}

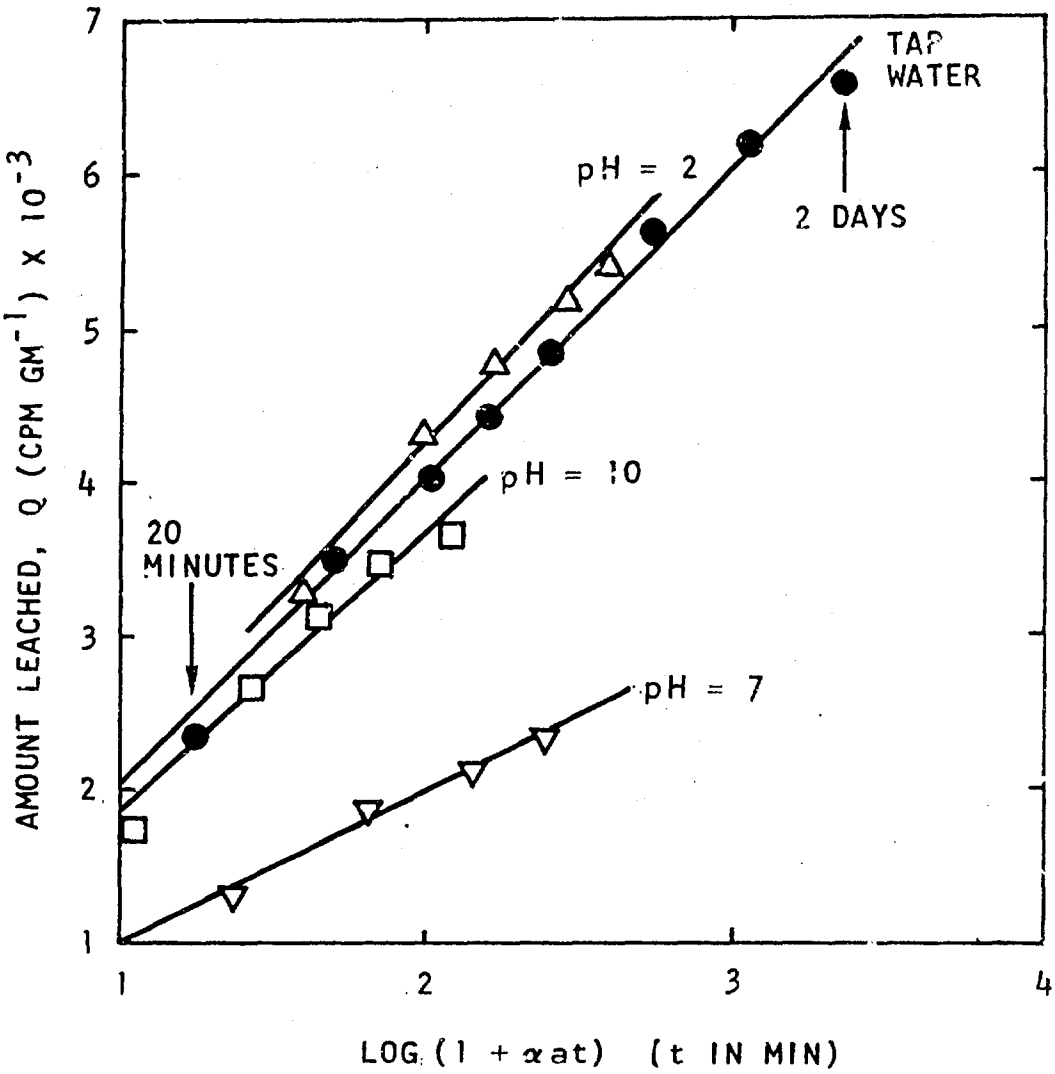

Fig. 35. Leaching of radioiodine from powdered 1450°K eutectic $CaO-Al_2O_3-SiO_2$. The data have been fitted to the Elovich equation

since the 100-μ particles were leached a depth of about 0.1 μ during the tap water leach. The true leaching mechanism is not understood. Douglas and Raman,[26] for instance, found a change in leaching mechanism from $t^{1/2}$ to a linear time dependency for leaching of sodium and potassium from silicates. It also seems possible that the mechanism depends upon the species being leached. The pH dependence of leaching found in the present work is in good agreement with dependences found by other authors.[27,28]

FALLOUT PARTICLE STUDIES

The condensed-state, diffusion-limited model of fission product absorption during fallout formation suggests that the concentration gradients of some radionuclides are very sharp. This is the result expected for radiocesium, for example. The importance of diffusion seems to be confirmed by the cursory experiment described below.

Some large silicate fallout particles from shot Johnie Boy (supplied by USNRDL) were microscopically examined and divided into two sets: coated particles and uncoated particles. Three particles were selected from the uncoated set for an experiment. Their gross appearance was that of a somewhat inhomogeneous, dark glass with obvious nodules of white material on the surface. Radii, r_o, were about 0.05 cm. The presence of radiocesium in the particles was established by gamma analysis using a multichannel analyser and a Cs^{137} standard for reference. After the particles were leached for 1 hr with 19% HCl, no significant loss of cesium was observed. Leaching studies were then made using 5% HF with subsequent washing, drying at 110°C for 1 hr, gamma analysis, and weighing on a microbalance. Microscopic examination of the particles throughout this process showed a continuous, but not uniform, radial attack. The experiment was concluded when the specimens lost their integrity. Results obtained in this experiment are shown in Table 6 where the

relative average concentration, $\overline{C}$, of cesium in the leached section is presented according to a calculated average radius, r, given by the weight loss. A concentration gradient is apparent in this table. Although this gradient seems small compared with the model calculations, if a uniform attack is assumed, it appears basically to support the model phenomenology.

Table 6

COMPOSITE Cs^{137} PROFILES IN THREE JOHNIE BOY PARTICLES

r/r_f	$K\overline{C}$
0.973	3.4
0.921	1.8
0.880	1.6

CLOUD CHEMISTRY PHENOMENOLOGY

Since its inception at General Atomic, the present program has had as a goal the understanding and simulation of nuclear cloud chemistry. Studies have included measurements of the thermodynamics of condensed and gaseous phases, condensed state diffusivities, and elemental distributions in fallout. Investigations have been made of the kinetic processes--agglomeration, condensation, and gaseous diffusion. Also, the reported mathematical fallout chemistry model has been constructed as a portion of this program.

These same phenomena appear to be the most important for future study. The proposed calculational model requires testing against fallout observational information, the effects of other phenomena must be evaluated critically, and further input information is needed to permit the appropriate calculations.

REFERENCES

1. Norman, J. H., and W. E. Bell, "Fallout Studies, High Temperature Interactions Between Gaseous Fission Products and Liquid Silicates," Final Report, Office of Civil Defense Report GA-4278, General Atomic Division, General Dynamics Corporation, May 24, 1963
2. Norman, J. H. et al., "Fallout Studies, Cloud Chemistry," Final Report, Office of Civil Defense Report GA-6094, General Atomic Division, General Dynamics Corporation, 1965.
3. Norman, J. H., and P. Winchell, "Cloud Chemistry of Fallout Formation" in Proceedings/Part 1, Fallout Phenomena Symposium, U. S. Naval Radiological Defense Laboratory Report No. USNRDL-R & L-177, June 1966.
4. Merten, U., J. Phys. Chem. 63, 443 (1959).
5. Norman, J., "Henry's Law Constants for Dissolution of Fission Products in a Silicate Fallout Particle Matrix," U. S. Naval Radiological Defense Laboratory Report GA-7058, General Atomic Division, General Dynamics Corporation, 1966.
6. Korts, R. F., and J. H. Norman, "A Calculational Model for Condensed State Diffusion Controlled Fission Product Absorption During Fallout Formation," U. S. Naval Radiological Defense Laboratory Report GA-7598, General Atomic Division, General Dynamics Corporation, 1966.

6a. Dixon, W. J., and F. J. Massey, Introduction to Statistical Analysis, McGraw-Hill Book Company, Inc., New York, 1951.

7. Shewmon, P. G., Diffusion in Solids, McGraw-Hill Book Company, Inc., New York, 1963.
8. Rüetschi, P., Z. Physik. Chem. 14, 277 (1958).
9. Levi, D. L., Discussions Farad. Soc. 42A, 152 (1946).
10. Cartledge, G. H., J. Am. Chem. Soc. 52, 3076 (1930).

11. Ralkova, J., Silikaty 6, 258 (1962).

12. Norman, J. H., and H. G. Staley, "Knudsen Cell Measurements to Determine the Stabilities of Gaseous Cesium and Rubidium Oxides," Proceedings of the Fourteenth Annual Conference on Mass Spectrometry and Allied Topics, Dallas, Texas, May 22-27, 1966 (to be published).

13. Brewer, L., and D. F. Mastick, J. Am. Chem. Soc. 73, 2045 (1951).

14. Klemm, V. W., and H. J. Scharf, Z. Anorg. Allgem. Chem. 303, 236 (1960).

15. White, D., et al., J. Chem. Phys. 39, 2463 (1963).

16. Norman, J. H., and H. G. Staley, "Stability of the Gaseous Alkali Metal Oxides," General Atomic Report (to be issued).

17. White, D., et al., Thermodynamics of Vaporization of Nuclear Materials, International Atomic Energy Agency, Vienna, 1962.

18. Miller, C. F., "Fallout and Radiological Countermeasures," Vol. I, Stanford Research Institute Project No. IM-4021, 1963.

19. Crocker, G. R., "Estimates of Fission Product Yields of a Thermonuclear Explosion," U. S. Naval Radiological Defense Laboratory Report USNRDL-TR-642, 1963.

20. Crocker, G. R., R. C. Scheidt, and M. D. Connors, "Radionuclide Input Data for Fission Product Abundance Computations," U. S. Naval Radiological Defense Laboratory Report USNRDL-TM-137, 1963.

21. Levin, E. M., C. R. Robbins, and H. F. McMurdie, Phase Diagrams for Ceramists, The American Ceramic Society, Columbus, Ohio, 1964.

22. Low, M. J. D., Chem. Rev. 60, 267 (1960).

23. Ralkova, J., and J. Saidl in Treatment and Storage of High-Level Radioactive Wastes, International Atomic Energy Agency, Vienna, 1963, p. 347.

24. Bonniaud, R., C. Sombret, and F. Laude, ibid., pp. 366-368, 372-373.

25. Clark, W. E., and H. W. Godbee, ibid, p. 430.

26. Hardwick, W. H., ibid., p. 353.

27. Ralkova, J., and J. Saidl, ibid., p. 344.

28. Voldan, J., and M. Palecek, Silikaty 1, 297 (1957).

UNCLASSIFIED
Security Classification

DOCUMENT CONTROL DATA - R&D

(Security classification of title, body of abstract and indexing annotation must be entered when the overall report is classified)

1. ORIGINATING ACTIVITY (Corporate author)	2a. REPORT SECURITY CLASSIFICATION
General Atomic Division General Dynamics Corporation San Diego, California	Unclassified
	2b. GROUP

3. REPORT TITLE

CLOUD CHEMISTRY OF FALLOUT FORMATION
FINAL REPORT

4. DESCRIPTIVE NOTES (Type of report and inclusive dates)

5. AUTHOR(S) (Last name, first name, initial)

Norman, John H. and Winchell, Perrin

6. REPORT DATE	7a. TOTAL NO. OF PAGES	7b. NO. OF REFS
January 13, 1967	81	29

8a. CONTRACT OR GRANT NO.	9a. ORIGINATOR'S REPORT NUMBER(S)
N228-(62479)67968 and NOO22866C0403 b. PROJECT NO.	GA-7597
c.	9b. OTHER REPORT NO(S) (Any other numbers that may be assigned this report)
d.	

10. AVAILABILITY/LIMITATION NOTICES

Each transmittal of this document outside agencies of the U.S. Government must have prior approval of the Office of Civil Defense, Office of Secretary of Army.

11. SUPPLEMENTARY NOTES	12. SPONSORING MILITARY ACTIVITY
	Office of Civil Defense, Office of the Secretary of the Army, Washington, D.C. 20310

13. ABSTRACT

A transpiration method was used to measure Henry's law constants as a function of temperature for cesium and rubidium dissolved in eutectic $CaO-Al_2O_3-SiO_2$. Diffusivities of cesium, rubidium, potassium, sodium, indium, tin, and iodine in this matrix and other matrices were determined with either a vaporization method or a plane source-sectioning method. Results of calculations obtained by using Henry's law constant absorption, condensed state diffusion-controlled calculational model for fission product distribution in fallout are presented. This scheme leads to the conclusion that fission product fractionation is mainly a property of the fallout particle size distribution and the particle sizes under consideration. Also, deviations of these calculations from the Miller-model type of calculation are considered. The stabilities of the alkali metal oxides as determined by Knudsen cell-mass spectrometric techniques are reported. The species $Cs_2O(g)$ and $Cs_2O_2(g)$, in particular, exhibit a much higher degree of stability than has been supposed. Electron microprobe studies of particles from a seeded Eniwetok detonation are described. Thermal and chemical histories of some particles are traced through dendritic forms, accretion events, occurrence of the seeding elements, etc. Results of some leaching studies, as they pertain to the condensed state diffusion-controlled, fission product absorption model, are presented.

DD FORM 1 JAN 64 1473

UNCLASSIFIED
Security Classification

14. KEY WORDS	LINK A		LINK B		LINK C	
	ROLE	WT	ROLE	WT	ROLE	WT
Henry's law constants						
Fallout formation						
Thermodynamics						
Fission products						
Transpiration						
Alkali metal oxides						
Diffusion						
Silicates						
Fallout						
Fallout model						
Leaching						
Electron microprobe						

INSTRUCTIONS

1. ORIGINATING ACTIVITY: Enter the name and address of the contractor, subcontractor, grantee, Department of Defense activity or other organization *(corporate author)* issuing the report.

2a. REPORT SECURITY CLASSIFICATION: Enter the overall security classification of the report. Indicate whether "Restricted Data" is included. Marking is to be in accordance with appropriate security regulations.

2b. GROUP: Automatic downgrading is specified in DoD Directive 5200.10 and Armed Forces Industrial Manual. Enter the group number. Also, when applicable, show that optional markings have been used for Group 3 and Group 4 as authorized.

3. REPORT TITLE: Enter the complete report title in all capital letters. Titles in all cases should be unclassified. If a meaningful title cannot be selected without classification, show title classification in all capitals in parenthesis immediately following the title.

4. DESCRIPTIVE NOTES: If appropriate, enter the type of report, e.g., interim, progress, summary, annual, or final. Give the inclusive dates when a specific reporting period is covered.

5. AUTHOR(S): Enter the name(s) of author(s) as shown on or in the report. Enter last name, first name, middle initial. If military, show rank and branch of service. The name of the principal author is an absolute minimum requirement.

6. REPORT DATE: Enter the date of the report as day, month, year; or month, year. If more than one date appears on the report, use date of publication.

7a. TOTAL NUMBER OF PAGES: The total page count should follow normal pagination procedures, i.e., enter the number of pages containing information.

7b. NUMBER OF REFERENCES: Enter the total number of references cited in the report.

8a. CONTRACT OR GRANT NUMBER: If appropriate, enter the applicable number of the contract or grant under which the report was written.

8b, 8c, & 8d. PROJECT NUMBER: Enter the appropriate military department identification, such as project number, subproject number, system numbers, task number, etc.

9a. ORIGINATOR'S REPORT NUMBER(S): Enter the official report number by which the document will be identified and controlled by the originating activity. This number must be unique to this report.

9b. OTHER REPORT NUMBER(S): If the report has been assigned any other report numbers *(either by the originator or by the sponsor)*, also enter this number(s).

10. AVAILABILITY/LIMITATION NOTICES: Enter any limitations on further dissemination of the report, other than those imposed by security classification, using standard statements such as:

(1) "Qualified requesters may obtain copies of this report from DDC."

(2) "Foreign announcement and dissemination of this report by DDC is not authorized."

(3) "U. S. Government agencies may obtain copies of this report directly from DDC. Other qualified DDC users shall request through _____."

(4) "U. S. military agencies may obtain copies of this report directly from DDC. Other qualified users shall request through _____."

(5) "All distribution of this report is controlled. Qualified DDC users shall request through _____."

If the report has been furnished to the Office of Technical Services, Department of Commerce, for sale to the public, indicate this fact and enter the price, if known.

11. SUPPLEMENTARY NOTES: Use for additional explanatory notes.

12. SPONSORING MILITARY ACTIVITY: Enter the name of the departmental project office or laboratory sponsoring *(paying for)* the research and development. Include address.

13. ABSTRACT: Enter an abstract giving a brief and factual summary of the document indicative of the report, even though it may also appear elsewhere in the body of the technical report. If additional space is required, a continuation sheet shall be attached.

It is highly desirable that the abstract of classified reports be unclassified. Each paragraph of the abstract shall end with an indication of the military security classification of the information in the paragraph, represented as *(TS), (S), (C), or (U)*.

There is no limitation on the length of the abstract. However, the suggested length is from 150 to 225 words.

14. KEY WORDS: Key words are technically meaningful terms or short phrases that characterize a report and may be used as index entries for cataloging the report. Key words must be selected so that no security classification is required. Identifiers, such as equipment model designation, trade name, military project code name, geographic location, may be used as key words but will be followed by an indication of technical context. The assignment of links, rules, and weights is optional.